

NOS Experimental Galveston Bay Nowcast/Forecast System: SF₆ Tracer Studies

Silver Spring, Maryland
June 2007



noaa National Oceanic and Atmospheric Administration

U.S. DEPARTMENT OF COMMERCE
National Ocean Service
Coast Survey Development Laboratory

**Office of Coast Survey
National Ocean Service
National Oceanic and Atmospheric Administration
U.S. Department of Commerce**

The Office of Coast Survey (OCS) is the Nation's only official chartmaker. As the oldest United States scientific organization, dating from 1807, this office has a long history. Today it promotes safe navigation by managing the National Oceanic and Atmospheric Administration's (NOAA) nautical chart and oceanographic data collection and information programs.

There are four components of OCS:

The Coast Survey Development Laboratory develops new and efficient techniques to accomplish Coast Survey missions and to produce new and improved products and services for the maritime community and other coastal users.

The Marine Chart Division acquires marine navigational data to construct and maintain nautical charts, Coast Pilots, and related marine products for the United States.

The Hydrographic Surveys Division directs programs for ship and shore-based hydrographic survey units and conducts general hydrographic survey operations.

The Navigational Services Division is the focal point for Coast Survey customer service activities, concentrating predominately on charting issues, fast-response hydrographic surveys, and Coast Pilot updates.

NOS Experimental Galveston Bay Nowcast/Forecast System: SF₆ Tracer Studies

Richard A. Schmalz, Jr.

**Office of Coast Survey, Coast Survey Development Laboratory, Silver Spring,
MD**

June 2007



noaa National Oceanic and Atmospheric Administration

**U. S. DEPARTMENT
OF COMMERCE**

Carlos Gutierrez, Secretary

**National Oceanic and
Atmospheric Administration**

**Conrad C. Lautenbacher, Jr.,
VADM USN (Ret.), Under Secretary**

**National Ocean Service
John H. Dunnigan**

Assistant Administrator

**Office of Coast Survey
Captain Steven R. Barnum, NOAA**

**Coast Survey Development Laboratory
Mary Erickson**

NOTICE

Mention of a commercial company or product does not constitute an endorsement by NOAA. Use for publicity or advertising purposes of information from this publication concerning proprietary products or the tests of such products is not authorized.

TABLE OF CONTENTS

LIST OF FIGURES	vi
LIST OF TABLES	viii
BASE MAP	ix
EXECUTIVE SUMMARY	x
1. INTRODUCTION	1
2. LONG WAVE HYDRODYNAMIC MODEL	3
2.1. Governing Equations	3
2.2. Model Grids	6
2.3. Air-Water Gas Transfer	6
3. SHORT WAVE HYDRODYNAMIC MODEL	11
3.1. Governing Equations	11
3.2. Initial Validation	11
3.3. Joint Computation	14
3.4. Refraction, Diffraction, and Reflection Limitations	14
4. WAVE-CURRENT INTERACTION	15
4.1. Surface Drag Coefficient Adjustment	15
4.2. Bottom Friction Adjustment	15
4.3. Surface Gas Transfer Velocity Adjustment	16
4.4. Wave Breaking Limitations	16
5. NOVEMBER 2004 SF6 TRACER SIMULATION	19
5.1. Set-Up	20
5.2. Long Wave Results	20
5.2.1. Water Surface Elevation	20
5.2.2. Prediction Depth Currents	20
5.2.3. Temperature	21
5.2.4. Salinity	21
5.3. Short Wave Results	33
5.3.1. Significant Wave Height	33
5.3.2. Wave Direction	33
5.3.3. Wave Period	33
5.4. SF ₆ Tracer Results	40
5.4.1. Concentration Fields	40
5.4.2. Residence Time	45
5.4.3. Exposure Level and Duration	45
5.4.4. Turnover Time	53
5.4.5. Mass Inventory	53
6. CONCLUSIONS AND FUTURE WORK	55
ACKNOWLEDGMENTS	55
REFERENCES	55

LIST OF FIGURES

Figure 1.1. Map showing Galveston Bay and the Houston Ship Channel including PORTS stations.....	2
Figure 2.1. Galveston Bay model grid.....	8
Figure 2.2. Galveston Bay model bathymetry, contours in meters.....	9
Figure 2.3. Houston Ship Channel model grid embedded in Bay model domain.	10
Figure 3.1. Galveston Bay wave model versus observed wave parameters at Eagle Point for January 25-30, 1997.....	12
Figure 3.2. Galveston Bay wave model versus observed wave parameters at 42035 for January 25-30, 1997.....	13
Figure 5.1. Patrick Bayou Superfund site. Injection site is at confluence of Patrick Bayou and the Houston Ship Channel.	19
Figure 5.2. Freshwater Inflows for the Trinity River, San Jacinto River, and Buffalo Bayou, November 1-12, 2004.....	22
Figure 5.3. Winds and sea level atmospheric pressure at Bolivar Roads, November 1-12, 2004.....	23
Figure 5.4. Winds and sea level atmospheric pressure at Eagle Point, November 1-12, 2004.....	24
Figure 5.5. Winds and sea level atmospheric pressure at Morgans Point, November 1-12, 2004.....	25
Figure 5.6. GBM simulated and observed water surface elevations at Galveston Pleasure Pier, Bolivar Roads, and Galveston Pier 21, November 1-12, 2004.....	26
Figure 5.7. HSCM simulated and observed water surface elevations at Eagle Point and Morgans Point and observed GBM water level residuals, November 1-12, 2004.....	27
Figure 5.8. GBM simulated and observed prediction depth currents at Bolivar Roads, November 1-12, 2004.....	28
Figure 5.9. HSCM simulated and observed prediction depth currents at Morgans Point, November 1-12, 2004.....	29
Figure 5.10. GBM simulated and observed temperature and surface salinity at Bolivar Roads, November 1-12, 2004.....	30
Figure 5.11. HSCM simulated and observed temperature and surface salinity at Eagle Point, November 1-12, 2004.....	31
Figure 5.12. HSCM simulated and observed temperature and surface salinity at Morgans Point, November 1-12, 2004.....	32
Figure 5.13. GBM and HSCM simulated significant wave height, November 1, 2004.....	34
Figure 5.14. GBM and HSCM simulated significant wave height, November 12, 2004.....	35
Figure 5.15. GBM and HSCM simulated significant wave direction, November 1, 2004.....	36
Figure 5.16. GBM and HSCM simulated significant wave direction, November 12, 2004.....	37

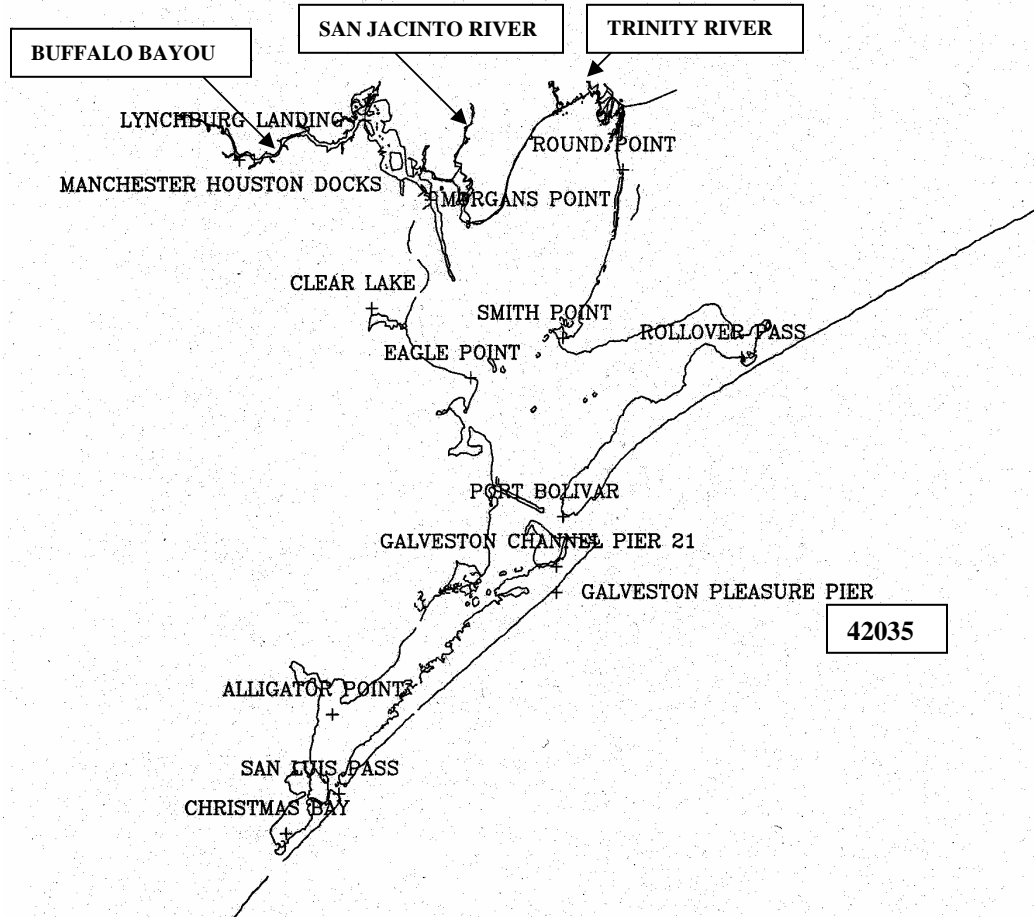
LIST OF FIGURES

Figure 5.17. GBM and HSCM simulated significant wave period, November 1, 2004.....	38
Figure 5.18. GBM and HSCM simulated significant wave period, November 12, 2004.....	39
Figure 5.19. GBM simulated near surface SF ₆ concentration at 00 CST on November 12, 2004 (Upper panel surface flux (CS1), Lower Panel no surface flux (CS2))	41
Figure 5.20. GBM simulated near bottom SF ₆ concentration at 00 CST on November 12, 2004 (Upper panel surface flux (CS1), Lower Panel no surface flux (CS2)).	42
Figure 5.21. HSCM simulated near surface SF ₆ concentration at 00 CST on November 12, 2004 (Upper panel surface flux (CS1), Lower Panel no surface flux (CS2))	43
Figure 5.22. HSCM simulated near bottom SF ₆ concentration at 00 CST on November 12, 2004 (Upper panel surface flux (CS1), Lower Panel no surface flux (CS2)).	44
Figure 5.23. GBM simulated near surface residence time (Upper panel surface flux (CS1), Lower Panel no surface flux (CS2)).....	46
Figure 5.24. GBM simulated near bottom residence time (Upper panel surface flux (CS1), Lower Panel no surface flux (CS2)).....	47
Figure 5.25. HSCM simulated near surface residence time (Upper panel surface flux (CS1), Lower Panel no surface flux (CS2)).....	48
Figure 5.26. HSCM simulated near bottom residence time (Upper panel surface flux (CS1), Lower Panel no surface flux (CS2)).....	49
Figure 5.27. Simulated near surface no surface flux (CS2) average exposure levels (fmol/L) (Upper panel GBM, Lower Panel HSCM)	50
Figure 5.28. Simulated near surface no surface flux (CS2) maximum exposure levels (fmol/L) (Upper panel GBM, Lower Panel HSCM)	51
Figure 5.29. Simulated near surface no surface flux (CS2) exposure duration (days) (Upper panel GBM, Lower Panel HSCM)	52

LIST OF TABLES

Table 5.1. SF ₆ Injection Characteristics at 00 CST on November 2, 2004. Note CS1 represents SF ₆ with gas transfer, while CS2 represents SF ₆ with no gas transfer.	20
Table 5.2. SF ₆ Turnover times (days). Note CS1 represents SF ₆ with gas transfer, while CS2 represents SF ₆ with no gas transfer and k=1 (surface),2,3,4, 5(bottom) sigma levels.	53
Table 5.3. GBM SF ₆ Mass inventory (10 ⁻³ fmoles). Initial mass at 00 CST on November 2, 2004 and final mass at 00CST on November 12, 2004. Note CS1 represents SF ₆ with gas transfer, while CS2 represents SF ₆ with no gas transfer	54
Table 5.4. HSCM SF ₆ Mass inventory (10 ⁻³ fmoles). Initial mass at 00 CST on November 2, 2004 and final mass at 00CST on November 12, 2004. Note CS1 represents SF ₆ with gas transfer, while CS2 represents SF ₆ with no gas transfer	54

GALVESTON BAY BASE MAP



Galveston Bay Base Map

EXECUTIVE SUMMARY

The Bay and Channel hydrodynamic models within the Galveston Bay Operational Forecast System (GBOFS) have been used to simulate the dispersion of a tracer in the Houston Ship Channel and upper Galveston Bay. With two concentration algorithms added to each model, the hydrodynamic model simulates the movement of the passive tracer sulfur hexafluoride (SF_6) with and without surface gas transfer over a ten day period, November 2-11, 2004. To accomplish this, GBOFS has been extended to enable a hindcast on demand capability for up to a one month duration.

The two hydrodynamic models have been set-up for simulating the tracer movement for a planned release of 1.0 mole of SF_6 at the confluence of Patrick Bayou and the Houston Ship Channel. The Bay model is forced with USGS river inflows, PORTS observed surface winds and PORTS water levels at Galveston Pleasure Pier at the lateral open boundaries, which extend to the 20m isobath in the near Gulf. The Bay model is one-way coupled to the Channel model, which is also forced with USGS river inflows and PORTS observed surface winds. Discharges at the Trinity River, San Jacinto River, and Buffalo Bayou are considered as a one-dimensional inflow with a zero input of tracer. The simulated water levels, currents, and density are validated with PORTS observations to ensure model accuracy. Model simulated tracer concentration distributions and the total tracer mass balance are studied and were used to design the May 17 - 27, 2005 field experiment conducted by Columbia University. The areal extent of the 10 day residence time contours for both flux and no flux SF_6 conditions were used to determine the necessary extent of boat survey coverage. While the actual survey was conducted in May 2005 and the numerical simulations were for November 2004, the numerical and experimental residence time estimates were very similar and demonstrated the utility of the numerical models in planning actual tracer release field studies.

In addition, surface gravity wave algorithms have been incorporated in both hydrodynamic models to simulate short period waves with and without wave-current interaction. Results presented indicate the feasibility of including the wave algorithms within GBOFS. Recommendations for additional SF_6 simulation and wave-current interaction experiments are presented.

1. INTRODUCTION

Recently attention has been focused on investigating the computation of residence time in estuaries and bays via multi-dimensional numerical modeling to aid in NOAA-EPA exposure assessment studies. In conjunction with a NOS Partnership Project, a workshop was held in June 2004 (NOS, 2005) to further study the problem. One area of application was the Houston Ship Channel and the potential for toxic releases from the EPA Superfund site at Patrick Bayou. Wei (2004) has studied the transport of sulfur hexafluoride (SF_6) within New York Harbor using the New York Harbor Operational Forecast System (NYOFS) model. Here, we attempt to build on this work and investigate the transport of SF_6 within the Houston Ship Channel and Galveston Bay.

Galveston Bay (Figure 1.1) has a complex geometry with the Houston Ship Channel bisecting the Bay and connecting the Port of Houston to the near Gulf. The Houston Ship Channel is important for both safe navigation and hydrodynamics in the Bay. Tidal currents through the channel play an important role in determining the dispersion characteristics. Flows from Buffalo Bayou, the San Jacinto River (Lake Houston Dam), and the Trinity River provide freshwater to Galveston Bay. These river inflows interact with the tidal currents to further complicate the circulation and transport in Galveston Bay.

Columbia University researchers conducted a field experiment in the Houston Ship Channel to study the circulation, mixing, and the transport and the fate of solutes using SF_6 during the period 17-27 May 2005. Approximately 1.0 mol of SF_6 was injected in the Houston Ship Channel at Patrick Bayou (downstream of a EPA superfund site) and the SF_6 tracer was observed over the next 10 days using a high-resolution measurement system similar to that used in June 2003 in the East River, NY. Measured data were processed and compiled for dispersion characteristics interpretation (Schlosser et al., 2006). Detailed measurement system description and results from the NY study are described in Caplow et al. (2003).

NOAA's National Ocean Service (NOS) has developed the Galveston Bay Operational Forecast System (GBOFS) to simulate water levels, current velocities, and density for use by mariners navigating in Galveston Bay and the Houston Ship Channel (NOS, 1999; Schmalz, 1998b, 1998c; Schmalz, 2000a, 2000b; Schmalz and Richardson, 2002) based on the Princeton Ocean Model (POM, Blumberg and Mellor, 1987). This forecast system (Schmalz, 2004) has been running operationally since June 2004 utilizing the near real-time water level and current information from NOS' Physical Oceanographic Real-Time System (PORTS). The hydrodynamic models in this system have been used to simulate the SF_6 transport in the Houston Ship Channel and upper Galveston Bay during the ten day period 2-11 November 2004 to examine the dispersion characteristics of the upper Houston Ship Channel. Areal extents of tracer concentration above background levels of 2 fmol/L were computed for the case of zero and non-zero SF_6 surface fluxes and bracketed the areal extent of the measured SF_6 concentrations above background level measured. (Refer to Figure 3 in Appendix 3 of Schlosser et al., 2006) and demonstrated the ability of numerical models to assist in the planning of the tracer release experiments in Galveston Bay. This report documents the modeling work performed to simulate the transport of SF_6 . The model set-up, simulation procedures, and results are described. Conclusions and future work based on the simulation results are discussed.

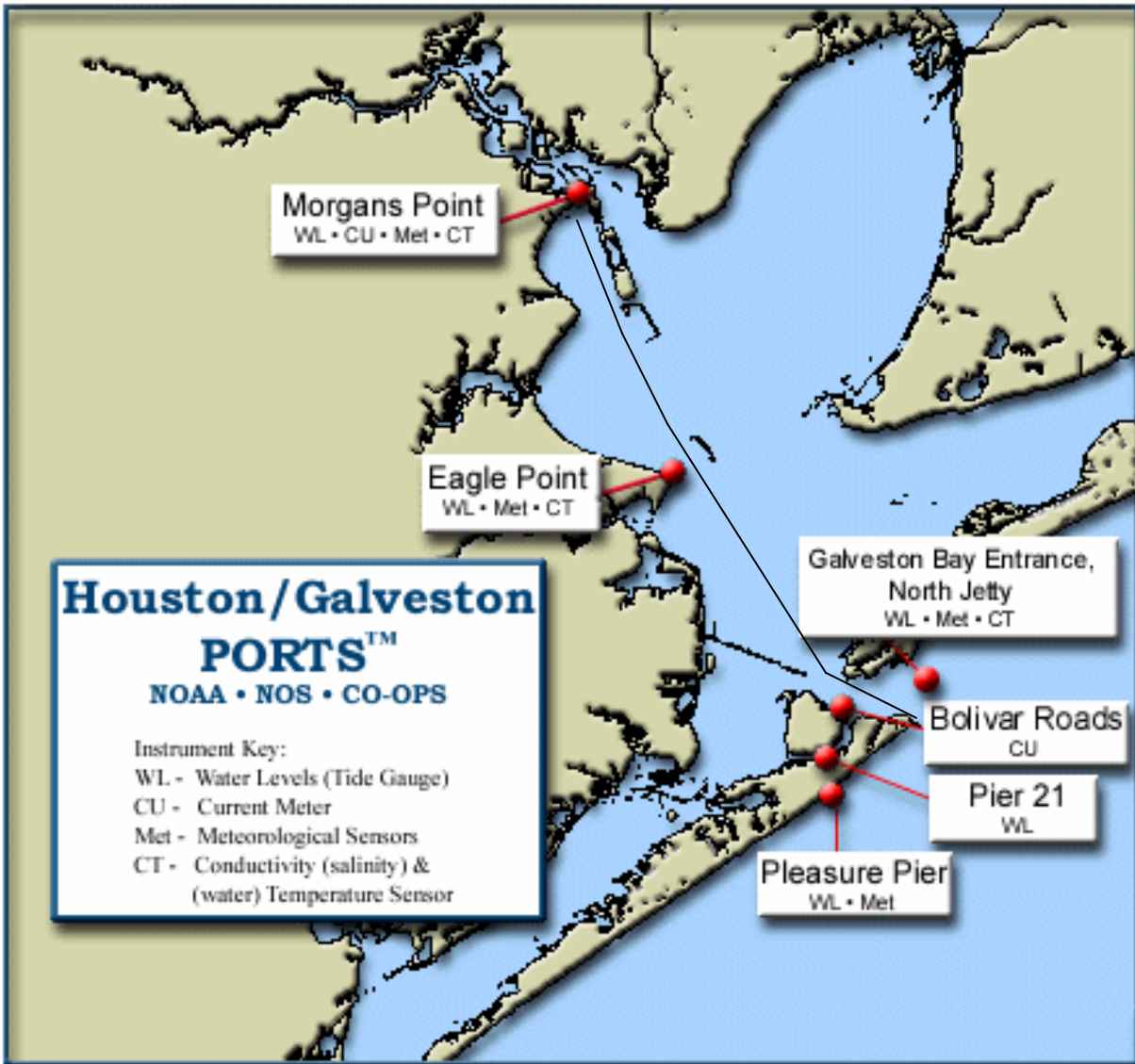


Figure 1.1. Map showing Galveston Bay and the Houston Ship Channel including PORTS stations.

2. LONG WAVE HYDRODYNAMIC MODEL

2.1. Governing Equations

A three-dimensional sigma coordinate Galveston Bay and near shelf model (GBM) has been developed (Schmalz, 1996) based on a version of the Blumberg and Mellor (1987) model extended to orthogonal curvilinear coordinates. GBM is a three-dimensional baroclinic circulation model, based on POM, for simulating water levels, current velocities, and density. The model is forced with: water levels at the near shore open boundaries based on observed levels at Galveston Pleasure Pier; freshwater inflows from the Buffalo Bayou, San Jacinto, and Trinity Rivers; and surface winds. In addition, a high resolution Houston Ship Channel model (HSCM) has been incorporated to provide finer spatial resolution (Schmalz, 1998a; 2000a; 2000c). The governing equations in a vertical sigma coordinate are briefly given as follows. Detailed formulation is contained in Blumberg and Mellor (1987), Mellor (2003b), and Schmalz (2001).

$$\mathfrak{I}(1) = 0, \quad (1)$$

$$\mathfrak{I}(U) - fDV + gD \frac{\partial \eta}{\partial x} = \frac{\partial}{\partial \sigma} \left[\frac{K_M}{D} \frac{\partial U}{\partial \sigma} \right] - \frac{gD^2}{\rho_0} \int_{\sigma}^0 \frac{\partial \rho}{\partial x} d\sigma + \frac{gD}{\rho_0} \frac{\partial D}{\partial x} \int_{\sigma}^0 \sigma \frac{\partial \rho}{\partial \sigma} d\sigma + F_x, \quad (2)$$

$$\mathfrak{I}(V) + fDU + gD \frac{\partial \eta}{\partial y} = \frac{\partial}{\partial \sigma} \left[\frac{K_M}{D} \frac{\partial V}{\partial \sigma} \right] - \frac{gD^2}{\rho_0} \int_{\sigma}^0 \frac{\partial \rho}{\partial y} d\sigma + \frac{gD}{\rho_0} \frac{\partial D}{\partial y} \int_{\sigma}^0 \sigma \frac{\partial \rho}{\partial \sigma} d\sigma + F_y, \quad (3)$$

$$\mathfrak{I}(T) = \frac{\partial}{\partial \sigma} \left[\frac{K_H}{D} \frac{\partial T}{\partial \sigma} \right] + F_T, \quad (4)$$

$$\mathfrak{I}(S) = \frac{\partial}{\partial \sigma} \left[\frac{K_H}{D} \frac{\partial S}{\partial \sigma} \right] + F_S, \quad (5)$$

$$\mathfrak{I}(q^2) = \frac{\partial}{\partial \sigma} \left[\frac{K_q}{D} \frac{\partial q^2}{\partial \sigma} \right] + \frac{2K_M}{D} \left[\left(\frac{\partial U}{\partial \sigma} \right)^2 + \left(\frac{\partial V}{\partial \sigma} \right)^2 \right] + \frac{2gK_H}{\rho_0} \frac{\partial \rho}{\partial \sigma} - \frac{2Dq^3}{B_1 l} + F_q, \quad (6)$$

$$\mathfrak{I}(q^2 l) = \frac{\partial}{\partial \sigma} \left[\frac{K_q}{D} \frac{\partial (q^2 l)}{\partial \sigma} \right] + E_1 l \left[\frac{K_M}{D} \left(\left(\frac{\partial U}{\partial \sigma} \right)^2 + \left(\frac{\partial V}{\partial \sigma} \right)^2 \right) + \frac{E_3 g}{\rho_0} K_H \frac{\partial \rho}{\partial \sigma} \right] - \frac{Dq^3}{B_1} \tilde{W} + F_l, \quad (7)$$

where $\mathfrak{I}(\ast) = \frac{\partial D \ast}{\partial t} + \frac{\partial UD \ast}{\partial x} + \frac{\partial VD \ast}{\partial y} + \frac{\partial \omega \ast}{\partial \sigma}$ and $\sigma = (z - \eta)/(H + \eta)$. Here (x, y, z, t) are the Cartesian

spatial and temporal coordinates and $D = H + \eta$ is the total water depth with H the depth and η the water surface elevation with respect to model datum. U and V are horizontal velocities, S and T are salinity and temperature, K_M and K_H are the vertical kinematic viscosity and diffusivity, respectively, K_q is vertical turbulence mixing coefficient, q^2 is twice the turbulence kinetic energy, and l is the turbulence length scale.

Note $\tilde{W} = 1 + E_2 \left(\frac{l}{\kappa L} \right)^2$, $\kappa = 0.4$ is the von Karman constant with $L^{-1} = (\eta - z)^{-1} + (H + z)^{-1}$, and B_1 , E_1 ,

E_2 , and E_3 are constants. g is the acceleration due to gravity, f is the Coriolis parameter, $\rho = \rho(S, T)$ is the water density, and ω is the transformed vertical velocity normal to a sigma surface. The relation of ω ($Hd\sigma/dt$) to the Cartesian vertical velocity w is

$$w = \omega + U \left[\sigma \frac{\partial D}{\partial x} + \frac{\partial \eta}{\partial x} \right] + V \left[\sigma \frac{\partial D}{\partial y} + \frac{\partial \eta}{\partial y} \right] + \sigma \frac{\partial D}{\partial t} + \frac{\partial \eta}{\partial t}. \quad (8)$$

The horizontal viscosity F_x and F_y and diffusion terms F_* are defined as

$$F_x = \frac{\partial}{\partial x} \left[2DA_M \frac{\partial U}{\partial x} \right] + \frac{\partial}{\partial y} \left[DA_M \left(\frac{\partial U}{\partial y} + \frac{\partial V}{\partial x} \right) \right] \quad (9)$$

$$F_y = \frac{\partial}{\partial y} \left[2DA_M \frac{\partial V}{\partial y} \right] + \frac{\partial}{\partial x} \left[DA_M \left(\frac{\partial U}{\partial y} + \frac{\partial V}{\partial x} \right) \right], \quad (10)$$

$$F_* = \frac{\partial}{\partial x} \left[DA_H \frac{\partial *}{\partial x} \right] + \frac{\partial}{\partial y} \left[DA_H \left(\frac{\partial *}{\partial y} \right) \right], \text{ with } * = (T, S, q, l, C) \quad (11)$$

where $A_M = A_H$ are the horizontal eddy viscosity and diffusivity, defined by the Smagorinsky formula (1963)

$$A_M = C_N \Delta x \Delta y \left[\left(\frac{\partial U}{\partial x} \right)^2 + 0.5 \left(\frac{\partial U}{\partial y} + \frac{\partial V}{\partial x} \right)^2 + \left(\frac{\partial V}{\partial y} \right)^2 \right]^{0.5}, \quad (12)$$

with C_N , a non-dimensional parameter.

For the passive tracer SF₆, the concentration equation is

$$\mathfrak{I}(C) = \frac{\partial}{\partial \sigma} \left[\frac{K_H}{D} \frac{\partial C}{\partial \sigma} \right] + F_C \quad (13)$$

where C is the concentration of SF₆.

Boundary conditions at the free surface ($\sigma=0$) are as follows:

$$\omega = 0, \rho \frac{K_M}{H} \left(\frac{\partial U}{\partial \sigma}, \frac{\partial V}{\partial \sigma} \right) = (\tau_{sx}, \tau_{sy}), \rho \frac{K_H}{H} \left(\frac{\partial S}{\partial \sigma}, \frac{\partial T}{\partial \sigma}, \frac{\partial C}{\partial \sigma} \right) = (\tilde{S}, \tilde{T}, \tilde{C}), l = 0, q^2 = B_1^{2/3} u_s^* \quad (14)$$

Boundary conditions at the bottom ($\sigma=-1$) are as follows:

$$\omega = 0, \rho \frac{K_M}{H} \left(\frac{\partial U}{\partial \sigma}, \frac{\partial V}{\partial \sigma} \right) = (\tau_{bx}, \tau_{by}), \rho \frac{K_H}{H} \left(\frac{\partial S}{\partial \sigma}, \frac{\partial T}{\partial \sigma}, \frac{\partial C}{\partial \sigma} \right) = (0, 0, 0), l = 0, q^2 = B_1^{2/3} u_b^* \quad (15)$$

where τ_s and τ_b are the wind stress and bottom friction and $(\tilde{S}, \tilde{T}, \tilde{C})$ are surface fluxes.

The above equation set is transformed into orthogonal horizontal coordinates after Blumberg and Herring (1987) with

$$dx = h_1 d\varepsilon_1, dy = h_2 d\varepsilon_2, ds^2 = dx^2 + dy^2 = h_1^2 d\varepsilon_1^2 + h_2^2 d\varepsilon_2^2 \text{ and } U_1 = h_1 \frac{d\varepsilon_1}{dt}, U_2 = h_2 \frac{d\varepsilon_2}{dt}.$$

$$\mathfrak{I}(1) = 0 \quad (16)$$

$$\mathfrak{I}(U_1) - \tilde{f} DU_2 + \frac{gD}{h_2} \frac{\partial \eta}{h_1 \partial \varepsilon_1} = \frac{K_M}{D} \frac{\partial}{\partial \sigma} \left[K_M \frac{\partial U_1}{\partial \sigma} \right] - \frac{gD}{\rho_0} \left[D \int_{\sigma}^0 \frac{\partial \rho}{h_1 \partial \varepsilon_1} d\sigma + \frac{\partial D}{h_1 \partial \varepsilon_1} \int_{\sigma}^0 \sigma \frac{\partial \rho}{\partial \sigma} d\sigma \right] + F_{12} \quad (17)$$

$$\mathfrak{I}(U_2) + \tilde{f} DU_1 + \frac{gD}{h_1} \frac{\partial \eta}{h_2 \partial \varepsilon_2} = \frac{K_M}{D} \frac{\partial}{\partial \sigma} \left[K_M \frac{\partial U_2}{\partial \sigma} \right] - \frac{gD}{\rho_0} \left[D \int_{\sigma}^0 \frac{\partial \rho}{h_2 \partial \varepsilon_2} d\sigma + \frac{\partial D}{h_2 \partial \varepsilon_2} \int_{\sigma}^0 \sigma \frac{\partial \rho}{\partial \sigma} d\sigma \right] + F_{21} \quad (18)$$

$$\mathfrak{I}(T) = \frac{\partial}{\partial \sigma} \left[\frac{K_H}{D} \frac{\partial T}{\partial \sigma} \right] + F_T \quad (19)$$

$$\mathfrak{I}(S) = \frac{\partial}{\partial \sigma} \left[\frac{K_H}{D} \frac{\partial S}{\partial \sigma} \right] + F_S \quad (20)$$

$$\mathfrak{I}(q^2) = \frac{\partial}{\partial \sigma} \left[\frac{K_q}{D} \frac{\partial q^2}{\partial \sigma} \right] + \frac{2K_M}{D} \left[\left(\frac{\partial U_1}{\partial \sigma} \right)^2 + \left(\frac{\partial U_2}{\partial \sigma} \right)^2 \right] + \frac{2gK_H}{\rho_0} \frac{\partial \rho}{\partial \sigma} - \frac{2Dq^3}{B_1 l} + F_q \quad (21)$$

$$\mathfrak{I}(q^2 l) = \frac{\partial}{\partial \sigma} \left[\frac{K_q}{D} \frac{\partial (q^2 l)}{\partial \sigma} \right] + E_1 l \left[\frac{K_M}{D} \left(\left(\frac{\partial U_1}{\partial \sigma} \right)^2 + \left(\frac{\partial U_2}{\partial \sigma} \right)^2 \right) + \frac{E_3 g}{\rho} K_H \frac{\partial \rho}{\partial \sigma} \right] - \frac{Dq^3}{B_1} \tilde{W} + F_l \quad (22)$$

where $\mathfrak{I}^* = \frac{\partial(D^*)}{\partial t} + \frac{\partial(h_2 U_1 D^*)}{h_1 h_2 \partial \varepsilon_1} + \frac{\partial(h_1 U_2 D^*)}{h_1 h_2 \partial \varepsilon_2} + \frac{\partial(\omega^*)}{\partial \sigma}$

$$\tilde{f} = f + \frac{U_2}{h_1 h_2} \frac{\partial h_2}{\partial \varepsilon_1} - \frac{U_1}{h_1 h_2} \frac{\partial h_1}{\partial \varepsilon_2}$$

The relationship of ω with the Cartesian vertical velocity w is

$$w = \omega + \frac{U_1}{h_2} \left[\sigma \frac{\partial D}{\partial \varepsilon_1} + \frac{\partial \eta}{\partial \varepsilon_1} \right] + \frac{U_2}{h_1} \left[\sigma \frac{\partial D}{\partial \varepsilon_2} + \frac{\partial \eta}{\partial \varepsilon_2} \right] + \sigma \frac{\partial D}{\partial t} + \frac{\partial \eta}{\partial t}. \quad (23)$$

The horizontal viscosity F_{ij} and diffusion terms F^* are defined as

$$F_{ij} = \frac{1}{h_i h_j} \left(\frac{\partial}{\partial \varepsilon_i} \left[2DA_M \frac{h_j \partial U_i}{h_i \partial \varepsilon_i} \right] + \frac{\partial}{\partial \varepsilon_j} \left[DA_M \left(\frac{h_i \partial U_i}{h_j \partial \varepsilon_j} + \frac{h_j \partial U_j}{h_i \partial \varepsilon_i} \right) \right] \right) \quad (24)$$

$$F^* = \frac{1}{h_1 h_2} \left(\frac{\partial}{\partial \varepsilon_1} \left[DA_H \frac{h_2 \partial^*}{h_1 \partial \varepsilon_1} \right] + \frac{\partial}{\partial \varepsilon_2} \left[DA_H \left(\frac{h_1 \partial^*}{h_2 \partial \varepsilon_2} \right) \right] \right), \text{ with } * = (T, S, q, l, C) \quad (25)$$

where

$$A_M = A_H = C_N h_1 h_2 \left[\left(\frac{\partial U_1}{\partial \varepsilon_1} \right)^2 + 0.5 \left(\frac{\partial U_1}{\partial \varepsilon_2} + \frac{\partial U_2}{\partial \varepsilon_1} \right)^2 + \left(\frac{\partial U_2}{\partial \varepsilon_2} \right)^2 \right]^{0.5}, \quad (26)$$

where C_N , a non-dimensional parameter, is set to be 0.005 for both Bay and Channel models.

For the passive tracer SF_6 , the concentration equation is

$$\mathfrak{I}(C) = \frac{\partial}{\partial \sigma} \left[\frac{K_H}{D} \frac{\partial C}{\partial \sigma} \right] + F_C \quad (27)$$

where C is the concentration of SF_6 .

Boundary conditions at the free surface ($\sigma=0$) and at the bottom ($\sigma=-1$) remain as given above,

while the concentration lateral open boundary condition during the outflow is specified with one-dimensional advection, $\frac{\partial(DC)}{\partial t} + \frac{\partial(DCU_i)}{h_i \partial \varepsilon_i} = 0$, where U_i is the velocity in the normal direction to the boundary while the following gradient condition is used for inflow, $\frac{\partial(DC)}{\partial t} = \frac{\partial(DCU_i)}{h_i \partial \varepsilon_i} = 0$.

2.2. Model Grids

The GBM computational grid as shown in Figure 2.1 consists of 181x101 horizontal cells ($dx = 254\text{-}2482\text{m}$, $dy = 580\text{-}3502\text{m}$) with 5 levels in the vertical. GBM water depths range from 1 m in the shallows to 20m along the shelf boundary. The HSCM grid shown in Figure 2.3 was developed in three sections. Each grid section was linked in order to develop the final composite channel grid consisting of 71 x 211 horizontal cells ($dx=63\text{-}1007\text{m}$, $dy=133\text{-}1268\text{m}$) with the same 5 sigma levels as in the GBM. Note navigation channel depths are order 14m. The two models were then nested in a one-way coupling scheme, wherein GBM water surface elevation, salinity, temperature, turbulent kinetic energy, and turbulent length scale time histories were saved at 6-minute intervals to provide boundary conditions to drive the HSCM. For salinity, temperature, turbulent kinetic energy, and turbulent length scale, a one-dimensional (normal to the boundary) advection equation is used. On inflow GBM values are advected into the HSCM domain, while on outflow HSCM internal values are advected through the boundary.

2.3. Air-Water Gas Transfer

After injection into the water column, part of the gaseous SF_6 tracer exits from the water into the air. The gas transfer velocity, k_{SF_6} , which measures the air-water SF_6 transfer rate, is determined based on k_{600} , the transfer velocity relative to a Schmidt Number of 600, which is determined based on a wind speed term (0.296 coefficient after Caplow et al., 2003) plus a temperature enhancement term reported by Wanninkhof (1992) as follows:

$$k_{600} = 0.296U_{10N}^2 + 2.5(0.5246 + 1.6256 \times 10^{-2} T_s + 4.9946 \times 10^{-4} T_s^2) \quad (28)$$

Next the Schmidt number, Sc , is computed as a function of temperature (0 to 30 °C) for salinity at 0 and 35 psu using the following relations given by Wanninkhof (1992):

$$\begin{aligned} Sc_0 &= 3255.3 - 217.13T_s + 6.8370T_s^2 - 0.086070T_s^3 \\ Sc_{35} &= 3531.6 - 231.40T_s + 7.2168T_s^2 - 0.090558T_s^3 \end{aligned} \quad (29)$$

The final transfer velocity, k_{SF_6} , is then determined after Ho et al. (2002) as follows:

$$k_{\text{SF}_6} = \frac{k_{600}}{\left(\frac{Sc_s}{600}\right)^n}, \text{ where } Sc_s, \text{ is the Schmidt number based on the surface salinity as determined}$$

from a linear interpolation from Sc_0 and Sc_{35} , and n is an exponent, which is set to 0.5 for no wave current interaction and is made a function of significant wave height, if wave current

interaction is considered (Jahne et al., 1987). The surface flux of SF₆, \tilde{C} , is then determined by:

$$\tilde{C} = k_{SF_6}(C_s - csol), \quad (30)$$

where C_s , is the surface SF₆ concentration, and $csol$ is the equilibrium solubility of SF₆, here taken as 2 fmol/L, as reported by Caplow et al. (2003).

GALVESTON BAY MODEL GRID

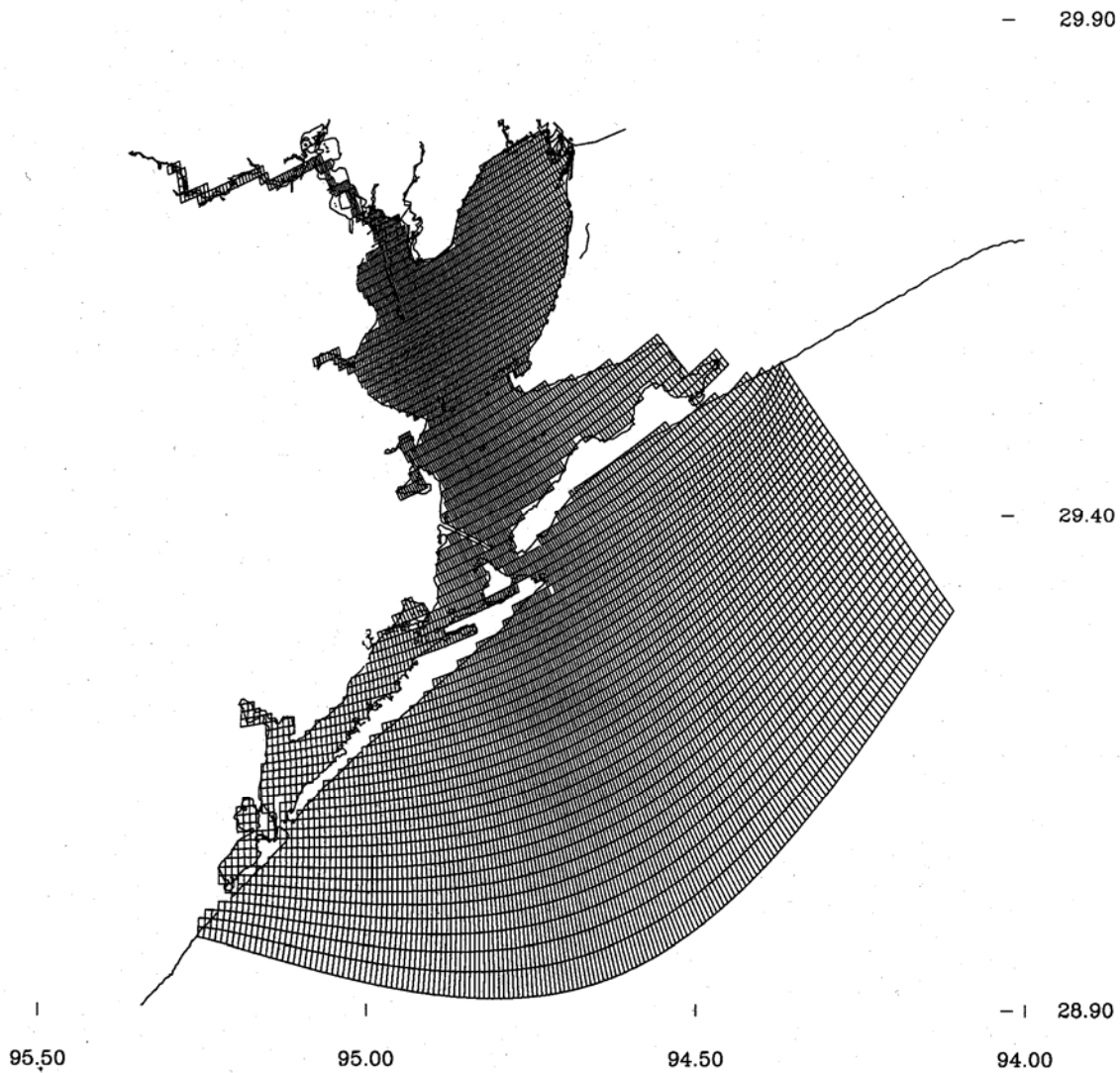


Figure 2.1. Galveston Bay/Houston Ship Channel model grid showing locations of water level gages and current meter.

GALVESTON BAY TOPOGRAPHY

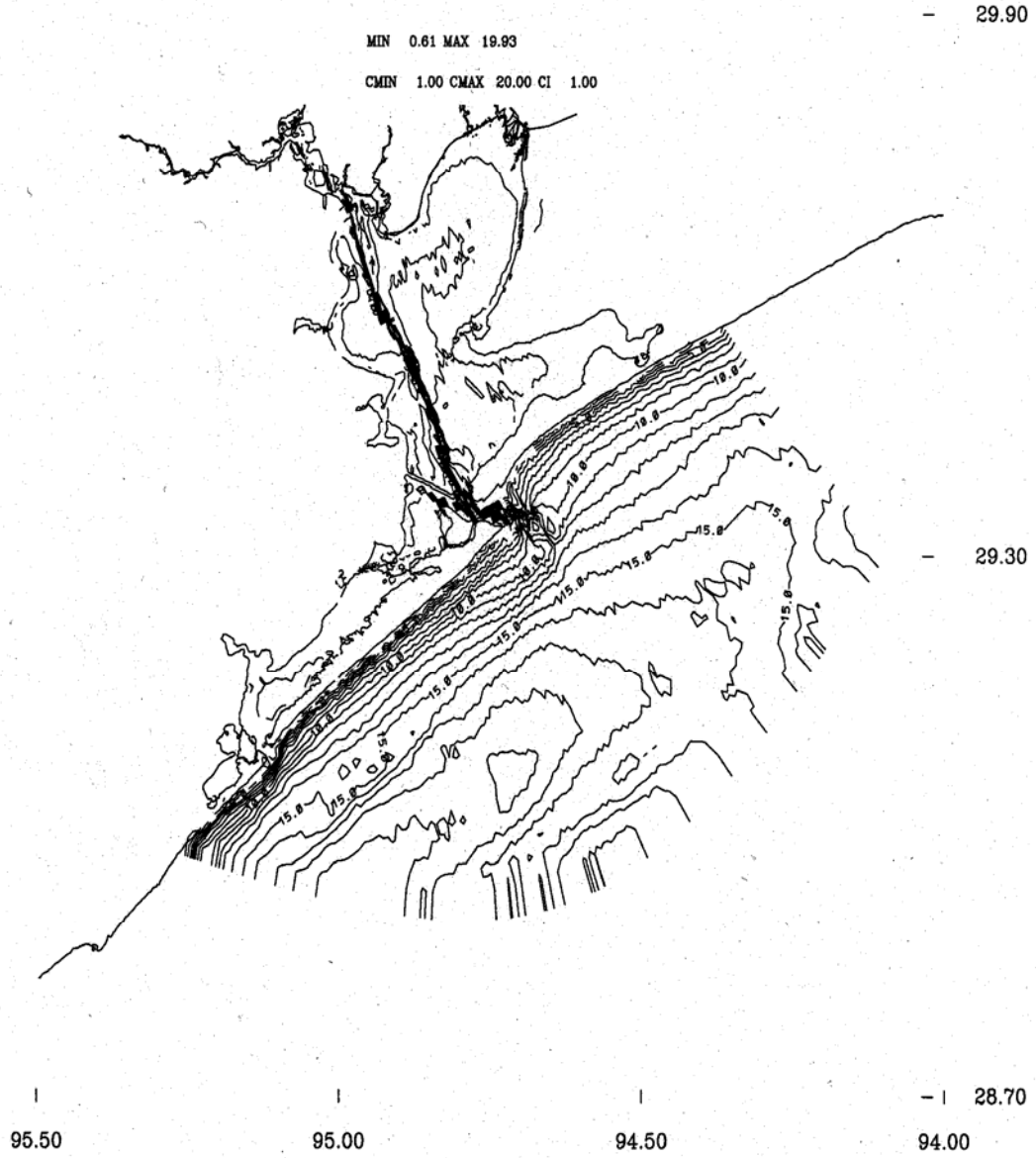


Figure 2.2. Galveston Bay model bathymetry, contours in meter.

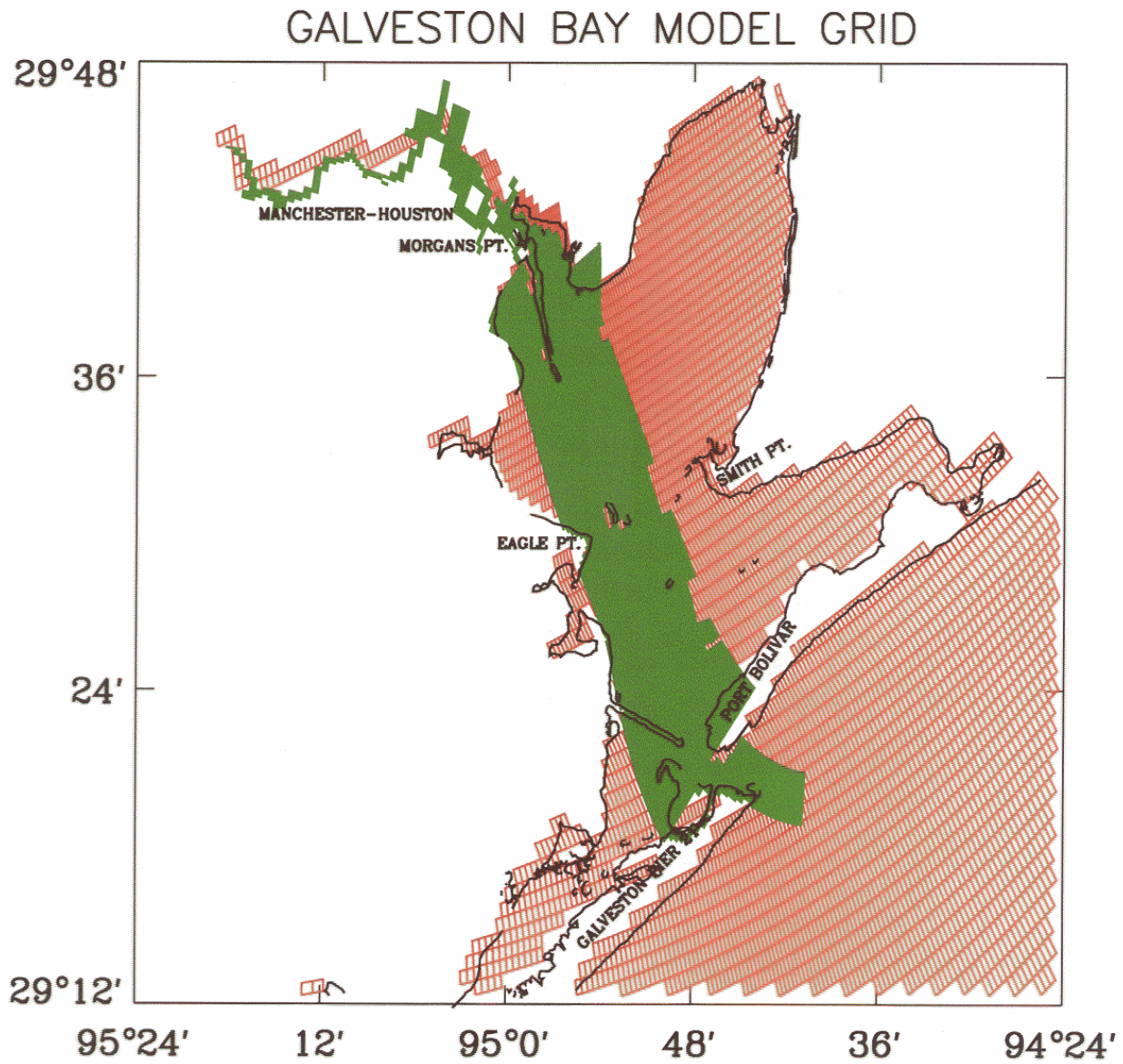


Figure 2.3. Galveston Bay model grid with Houston Ship Channel grid shown in green.

3. SHORT WAVE HYDRODYNAMIC MODEL

Schmalz (2003) has compared two USACE parametric wave models (CETN-I-6, 1981; Project CW-167, 1955) with the finite difference based Donelan (1977) wave model for wind events over Galveston Bay. The two parametric models considered were run on the same grid employed for the Bay circulation model (Figure 2.1), while a uniform square grid was used for the Donelan model. Further details on the Donelan (1977) wave model may be found in Schwab et al. (1984). Details of the initial testing may be found in Schmalz (2003). Best results as given in section 3.2 below were achieved by the following mixture of the two parametric models as presented in the governing equations below.

3.1. Governing Equations

CETN-I-6 (1981) significant wave height, H_s (ft):

$$\frac{gH_s}{U_A^2} = 0.283 \tanh[0.530[gD/U_A^2]^{0.75}] \tanh\left[\frac{0.00565[gF/U_A^2]^{0.5}}{\tanh[0.530[gD/U_A^2]^{0.75}]}\right] \quad (31)$$

CW-167 (Project CW-167, 1955): significant wave period, T_s (sec):

$$T_s = 6.262 \frac{U_A}{g} \left(\frac{gD}{U_A^2}\right)^{0.4507} \quad (32)$$

using the following notation:

g = Gravitational acceleration (32.2 ft/sec²)

U_A = Windspeed (kts)

F = Fetch (nm)

D = Total water depth (ft)

3.2. Initial Validation

The January 25-30, 1997 time period was studied due to the availability of USACE wave measurements off Eagle Point. Application of the models to this period revealed that despite the incorporation of shallow water effects in the finite difference based Donelan model by using a linear reduction in transfer of wind to wave momentum as described in Schmalz (2003), best results were achieved by using a combination of the two simpler parametric wave models. Total significant wave height was computed as the sum of the CETN-I-6 results plus the swell, which was determined at the open boundary from the NDBC Buoy 42035 measurements. The total significant wave period was taken as equal to the CW-167 result alone. Results for January 25-30, 1997 are shown in Figure 3.1 at Eagle Point and in Figure 3.2 at NDBC Buoy 42035, respectively. Note, the peak at Eagle Point is no longer delayed relative to the observations as experienced using the Donelan model with the shallow water adjustment and the peak at NDBC Buoy 42035 is well reproduced.

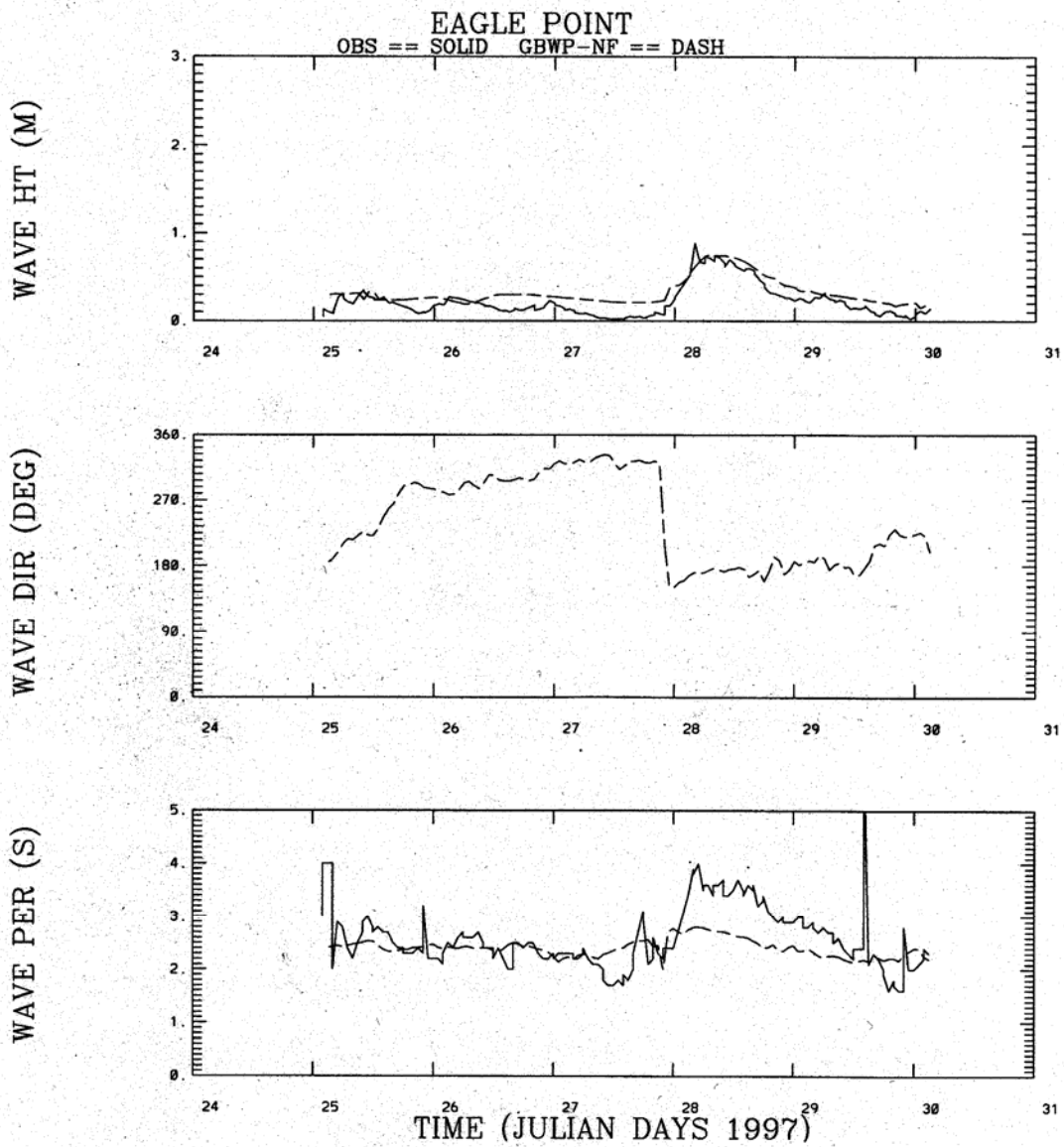


Figure 3.1. Galveston Bay Wave Model vs Observed Wave Parameters at Eagle Point, January 25-30 1997.

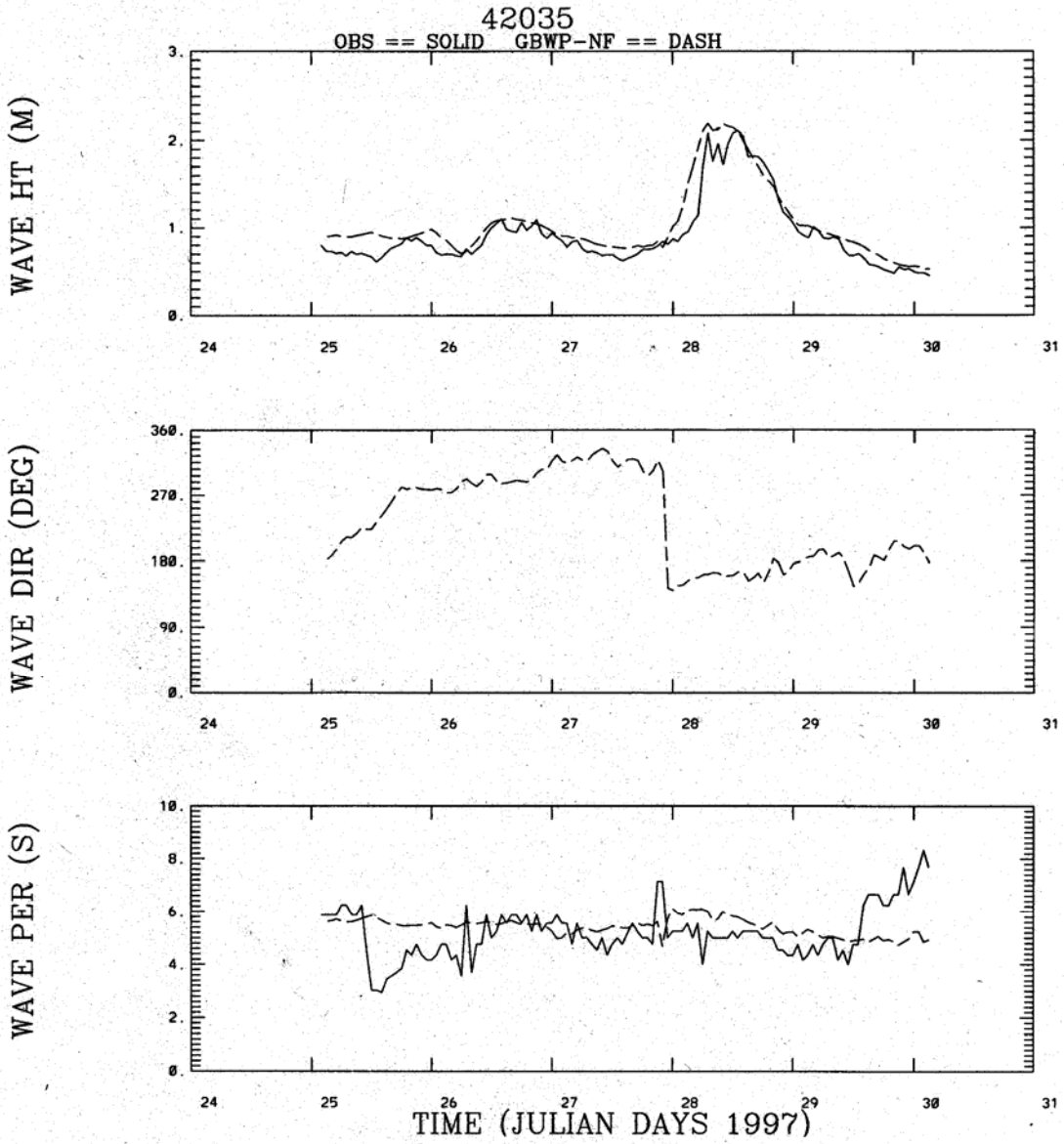


Figure 3.2. Galveston Bay Wave Model vs Observed Wave Parameters at 42035, January 25-30 1997.

3.3. Joint Computation

The mixed parametric wave model has been included as a subroutine within both the Bay and Channel long wave models and uses the same wind field. The waves are computed every six-minutes. In the Bay model, fetch data are specified for each octant of wind direction at 25 locations surrounding the Bay. An inverse distance squared interpolation is performed to determine the fetch distribution over the Bay for each wave computation. The long wave model provides the updated total water depth. At each wave computation in the Bay model, the swell height and fetch at each boundary point required by the Channel model are written on the transfer file in addition to the one-way coupled long wave information. Swell effects in the Bay model are input as a boundary condition and are reduced from the offshore boundary by a inverse distance squared interpolation of empirical reduction factors supplied at the above 25 locations around the Bay.

3.4. Refraction, Diffraction, and Reflection Limitations

Wave refraction due to changes in bathymetry is not specifically treated. The wave field is represented here by a single frequency, height, and direction rather than a continuous spectrum. Thus no wave-wave interaction is considered. Wave diffraction around breakwaters and jetties and wave reflection are also not included.

To include these three effects, a much more complicated and computationally intensive shallow water wave model must be included such as the Delft Technical University SWAN, which simulates the following physical phenomena: 1) wave generation and propagation in time and space, 2) shoaling, 3) refraction, 4) frequency shifting, 5) nonlinear wave-wave interactions, 6) whitecapping, and 7) blocking of waves by current. Note that diffraction and reflection are not explicitly modelled in SWAN but can be handled in the Delft Technical University PHAROS, a wave penetration finite element model. For further details refer to Rif (1997) for SWAN and Hurdle et al. (1989) for PHAROS.

As pointed out by Mellor and Donelan (2006), to perform shallow water wave computations with SWAN on the same grid as the POM circulation model a factor of 100 in computer time is needed. In practical applications, these computational requirements for shallow water wave computations are so severe that Mellor and Donelan (2006) advance a different initial approach.

4. WAVE-CURRENT INTERACTION MECHANICS

We consider a wave field with significant wave height, H_s , dominant period, C , and wave direction, ϕ . The wave direction is assumed to be in the direction of the wind. To determine the wave age, it is necessary to compute the wave phase speed, $C_p = \frac{\omega}{k}$, where $\omega = \frac{2\pi}{C}$, and

$k = \frac{\omega^2}{g \tanh(rk)}$, with $rk = \begin{cases} S(1 + 2e^{-2S} - 12e^{-4S}) & S > 2 \\ S^{0.5}(1 + 0.169S + 0.031S^2) & S \leq 2 \end{cases}$, where $S = D\omega^2 / g$ with D and g as defined previously as reported at http://web.mit.edu/fluids-modules/www/potential_flows/Lectures.

The friction velocity, u_* , is then computed as $u_* = U_{10N} \sqrt{C_{D10}}$, and the wave age is formed as the ratio of C_p to u_* .

4.1. Surface Drag Coefficient Adjustment

In the presence of waves, the surface drag coefficient is increased. Following Drennan et al. (2003), we employ their Figure 10 in which the drag coefficient, C_{D10N} , and wind speed, U_{10N} , are given versus inverse wave age, u_*/C_p . Wind speed ranges are from 5 to 20 m/s. The following relationships are used in the algorithm to define the adjustment factor of the surface drag, F , based the ratio of measured C_{D10N} with respect to inverse wave age to the Smith (1980) relationship.

$$\begin{aligned} F &= 1. - (0.16)(U_{10N} - 5)/15 & u_*/C_p \leq 0.06, \\ F &= 1.16 - (0.13)(U_{10N} - 5)/15 & 0.06 < u_*/C_p \leq 0.08, \\ F &= 1.27 - (0.07)(U_{10N} - 5)/15 & 0.08 < u_*/C_p \leq 0.10, \\ F &= 1.38 - (0.05)(U_{10N} - 5)/15 & 0.10 < u_*/C_p \end{aligned} \quad (34)$$

The effective surface drag coefficient, is given as the product of the adjustment factor, F , and the Large and Pond (1981) surface drag relation:

$$C_{D10N} \times 10^3 = \begin{cases} 1.2 & U_{10N} \leq 11 \text{ m/s} \\ (0.49 + 0.065U_{10N}) & U_{10N} > 11 \text{ m/s} \end{cases} \quad (35)$$

$$C_{eff} = FC_{D10N}$$

Note with no wave current interaction, $F=1.0$.

4.2. Bottom Friction Adjustment

In the presence of waves, the near bottom wave orbital velocity based on linear wave theory, U_o is first computed as $U_o = \frac{0.5H_s\omega}{\sinh(kD)}$ after Signell et al. (1990). The near bottom excursion

amplitude, a_b , and effective roughness, k_b , are then determined as $a_b = \frac{U_o}{\omega}$ and $k_b = 30z_0$, with z_0

the bottom roughness. The wave friction velocity, u_{*w} , is determined based on $S_b = k_b / a_b$ in the relationship reported by Grant and Madsen (1982) in the following manner:

$$f_w = \begin{cases} 0.13S_b^{0.40} & S_b < 0.08 \\ 0.23S_b^{0.62} & 0.08 \leq S_b \leq 1.0 \\ 0.23 & S_b > 1.0 \end{cases}, \text{ with } u_{*w} = \sqrt{0.5f_w U_o^2} \quad (36)$$

Next the current friction velocity, u_{*c} , is determined based on the model horizontal velocity components (U_b, V_b), at the level nearest the bed as follows (see Davies and Lawrence, 1995):

$$f_c = 2[\kappa / \ln(0.1/z_0)]^2, \text{ with } u_{*c} = \sqrt{0.5f_c (U_b^2 + V_b^2)} \quad (37)$$

The total friction velocity is then determined based on the current friction velocity and the wave friction velocity in the direction of the current as follows:

$$u_{*T} = \sqrt{u_{*c}^2 + (u_{*w} \cos(\theta_{wc}))^2}, \text{ where } \theta_{wc}, \text{ is the angle between the wave and wind directions (refer}$$

to Grant and Madsen, 1979). A roughness adjustment is determined as $F_p = \frac{24u_{*T}}{U_0} (S_b)^{1-\frac{u_{*c}}{u_{*T}}}$ as

reported by Signell (1990). The bottom friction adjustment factor, F_{pb} , is given

by $F_{pb} = \left[\frac{\ln(h_b / z_0)}{\ln(h_b / F_p z_0)} \right]^2$. In the present study, F_{pb} cannot exceed 2. The effective bottom

roughness is the product of the bottom roughness and this adjustment factor. Note in this approach, wave and current effects are considered independently (z_0 is never altered) and are then combined to determine the adjustment factor. In theory, an iterative approach on z_0 is desired.

4.3. Surface Gas Transfer Velocity Adjustment

Jahne et al. (1987) report that in the presence of waves on the surface, two important mechanisms are exhibited. First, the hydrodynamic boundary layer changes such that local divergences and convergences occur; this results in the exponent of the Schmidt number, n , decrease from 2/3 to 1/2. Second, additional energy is cycled with the energy gained by the waves being transferred to the near-surface turbulence. In our approach, the following relation is used to determine the Schmidt number exponent based on significant wave height.

$$\begin{aligned} n &= 0.667 & H_s &\leq 0.3 \\ n &= 0.60 & 0.3 < H_s &\leq 0.4 \\ n &= 0.55 & 0.4 < H_s &\leq 0.5 \\ n &= 0.50 & 0.5 < H_s & \end{aligned} \quad (38)$$

Note, for the case of no wave-current interaction, we still set $n=0.50$.

4.4. Breaking Wave Limitation

Within the context of the wave-current interaction algorithms considered above, wave breaking effects are not explicitly considered. Under the present approach, wave-current interactions act to increase surface and bottom stress, which leads to an increase in turbulence and enhanced vertical mixing. Mellor and Blumberg (2004) have considered wave breaking effects on the sea surface temperature. It would appear that additional research is needed on shallow water wave breaking effects and ultimately a shallow water wave and circulation model must be coupled. See Mellor and Donelan (2006) for one approach in this regard.

5. NOVEMBER 2004 SF₆ TRACER SIMULATION

A simulated release of SF₆ was conducted from November 2 to November 11, 2004. One mole was injected and assumed to be uniformly dissolved over the vertical at 00 CST on 2 November at the confluence of Patrick Bayou and the Houston Ship Channel (Figure 5.1). Note during the May 2005 experiment conducted by Columbia University approximately 1 mole of SF₆ was also injected at the same location as indicated in Appendix 2 of Schlosser et al. (2006). After the injection, the SF₆ tracer was then simulated over the next 10 days under the assumption of surface (CS1) and no surface gas (CS2) transfer. This was accomplished by using two separate concentration algorithms for CS1 and CS2. Detailed injection characteristics are given in Table 5.1. The Bay model long and short wave results were used to provide the boundary conditions for the finer resolution Houston Ship Channel simulation. Simulations were performed initially with no wave current interaction and are described here. Simulation results with wave-current interaction yielded essentially the same results, with a change in water surface elevations of order 0.5 cm.



Figure 5.1. Patrick Bayou Superfund site. Injection site is at the confluence of Patrick Bayou and the Houston Ship Channel

Table 5.1. SF₆ Injection Characteristics at 00 CST on November 2, 2004. Note CS1 represents SF₆ with surface gas transfer, while CS2 represents SF₆ with no surface gas transfer.

Parameter	Galveston Bay Model	Houston Ship Channel Model
Total Mass (moles)	1.0	1.0
(I,J) Grid Location	(50,88)	(31,178)
(DX,DY) grid spacings (m)	(378.0, 1043.9)	(213.8, 786.3)
Water depth with respect to model datum (m)	5.2	11.2
Total water depth (m)	5.5347	11.5452
Volume (m ³)	2,183,710	1,941,180
CS1 (k=1,5) (fmol/L)	457937	515151
CS2 (k=1,5) (fmol/L)	457937	515151

5.1. Set-Up

Observed river discharges for the Trinity River, San Jacinto, and Buffalo Bayou are shown in Figure 5.2 and exhibit relatively low flow conditions with a peak total flow of order 10,000 cfs on the 4 and 5 of November. Winds and atmospheric pressure as reported at the PORTS met stations shown at Bolivar Roads, Eagle Point, and Morgans Point in Figures 5.3-5.5, respectively, are uniform over the Bay with wind speeds order 10 to 12 kts. Water level residuals at Galveston Pleasure Pier are less than 25 cm, indicating a rather tranquil period.

The models were set up to simulate the SF₆ tracer concentration and to study the dispersion characteristics in the Houston Ship Channel and Upper Galveston Bay. The models simulated the water levels, currents, salinity, temperature, and SF₆ concentration with and without surface gas exchange from November 2 to November 12, 2004. The model was spun-up for one day from rest before the tracer injection at 00 UTC, November 2.

5.2. Long Wave Results

5.2.1. Water Surface Elevation

Simulated and observed water levels at Galveston Pleasure Pier, Bolivar Roads, and Galveston Pier 21, shown in Figure 5.6, indicate that the Bay model is accurately reproducing the water elevations at model interior locations. Water levels at Eagle Point and Morgans Point in Figure 5.7 indicate that the Channel model is also accurately reproducing the water elevations at model interior locations. Note the set-down of order 25cm during the period 3-8 November. In the first half of this period, the winds are from the North, and the Bay tends to empty with levels below the predicted astronomical tide.

5.2.2. Prediction Depth Currents

Simulated prediction depth currents at Bolivar Roads (Figure 5.8) from the Bay model and at Morgans Point (Figure 5.9) from the Channel model are in general agreement with the data. Note

the currents are bi-directional with strengths reduced as one proceeds from Bolivar Roads (125 cm/s) to Morgans Point (25-30 cm/s). Both models tend to slightly underestimate the peak currents with errors in direction of order 25 degrees.

5.2.3. Temperature

Temperature at Bolivar Roads (Figure 5.10) from the Bay model and at Eagle Point (Figure 5.11) and Morgans Point (Figure 5.12) from the Channel model are initialized to PORTS data. The initial SST field and boundary conditions are persisted over the 11 day period. This results in an error of order 5 °C by the end of the simulation period in sea surface temperature. Stratification at Bolivar Roads is underestimated during the 3-5 November period. A refinement to the set-up procedure would allow a linear increase or decrease of the initial climatological offshore boundary condition to be applied over the simulation.

5.2.4. Salinity

Surface salinity at Bolivar Roads (Figure 5.10) from the Bay model and at Eagle Point (Figure 5.11) and Morgans Point (Figure 5.12) from the Channel model are also initialized to PORTS data. No daily data assimilation of the PORTS salinity are performed. A persistence of the climatological boundary condition is used. Note in Figure 5.10 at Bolivar Roads, the presence of many lows in the observed time series, due to the advection of large gradients. Without data assimilation the errors in surface salinity are order 5 psu at the end of the 11 day simulation period. The above linear adjustment to the climatological offshore boundary condition would improve the salinity results as well

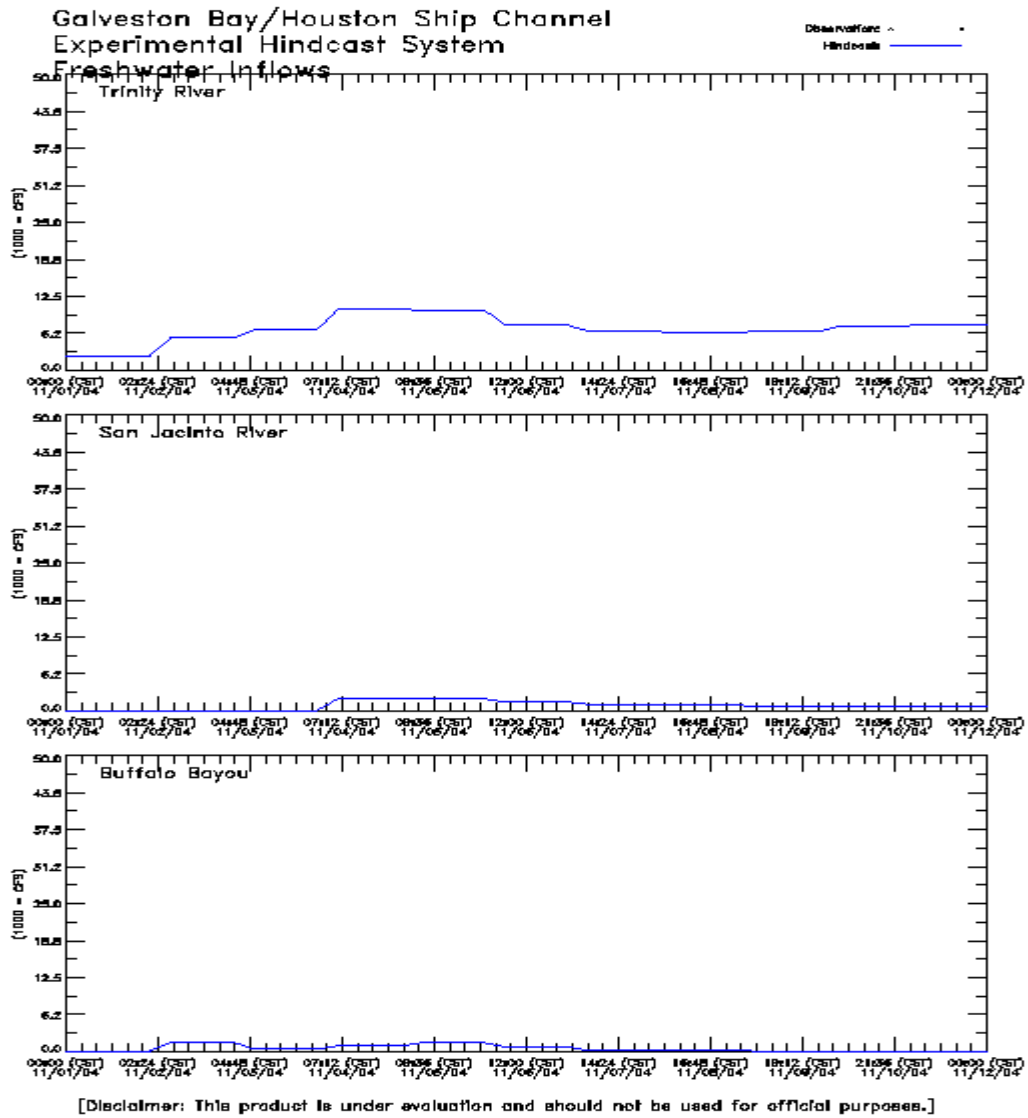


Figure 5.2. Freshwater Inflows for the Trinity River, San Jacinto River, and Buffalo Bayou, November 1-12, 2004.

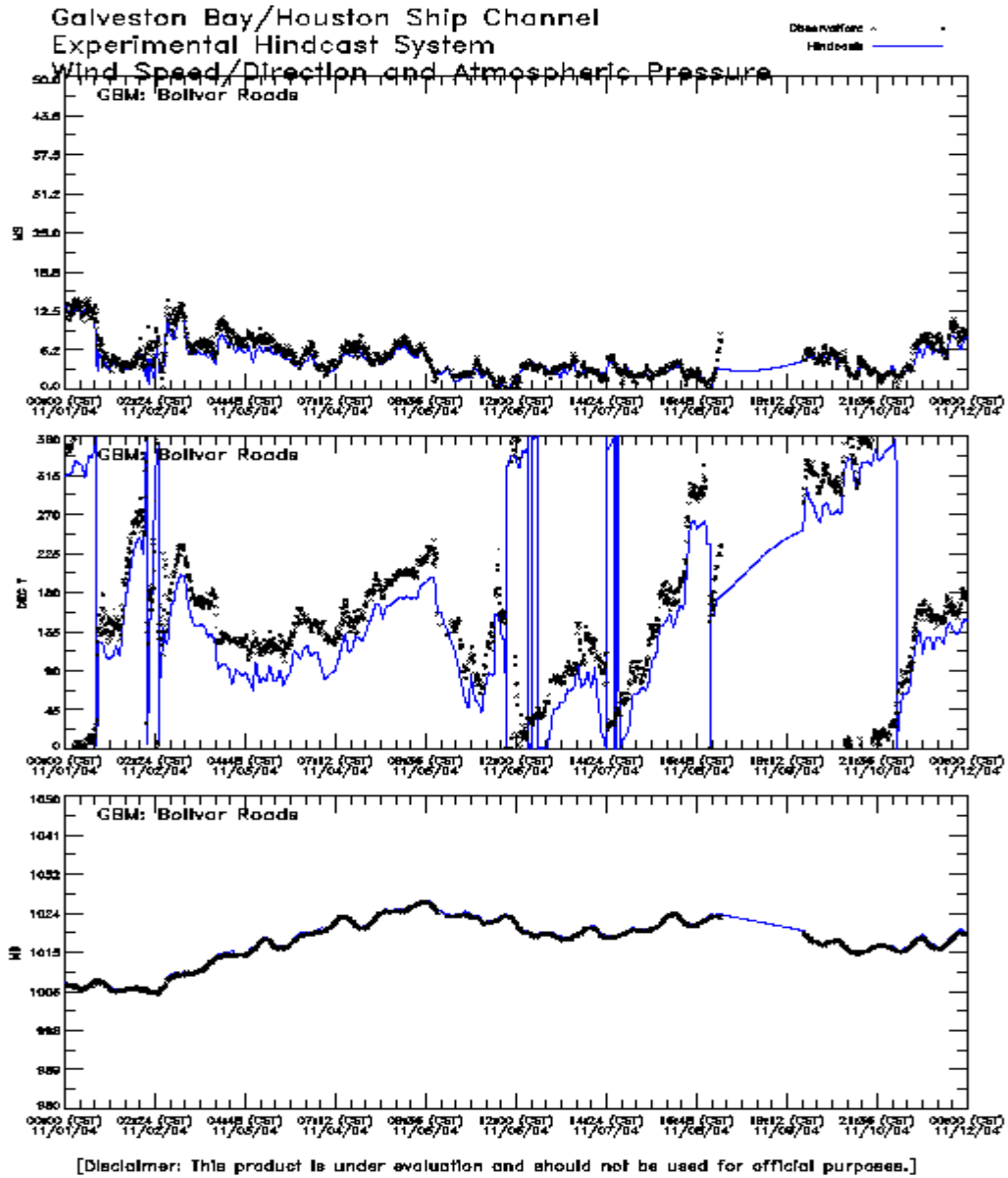
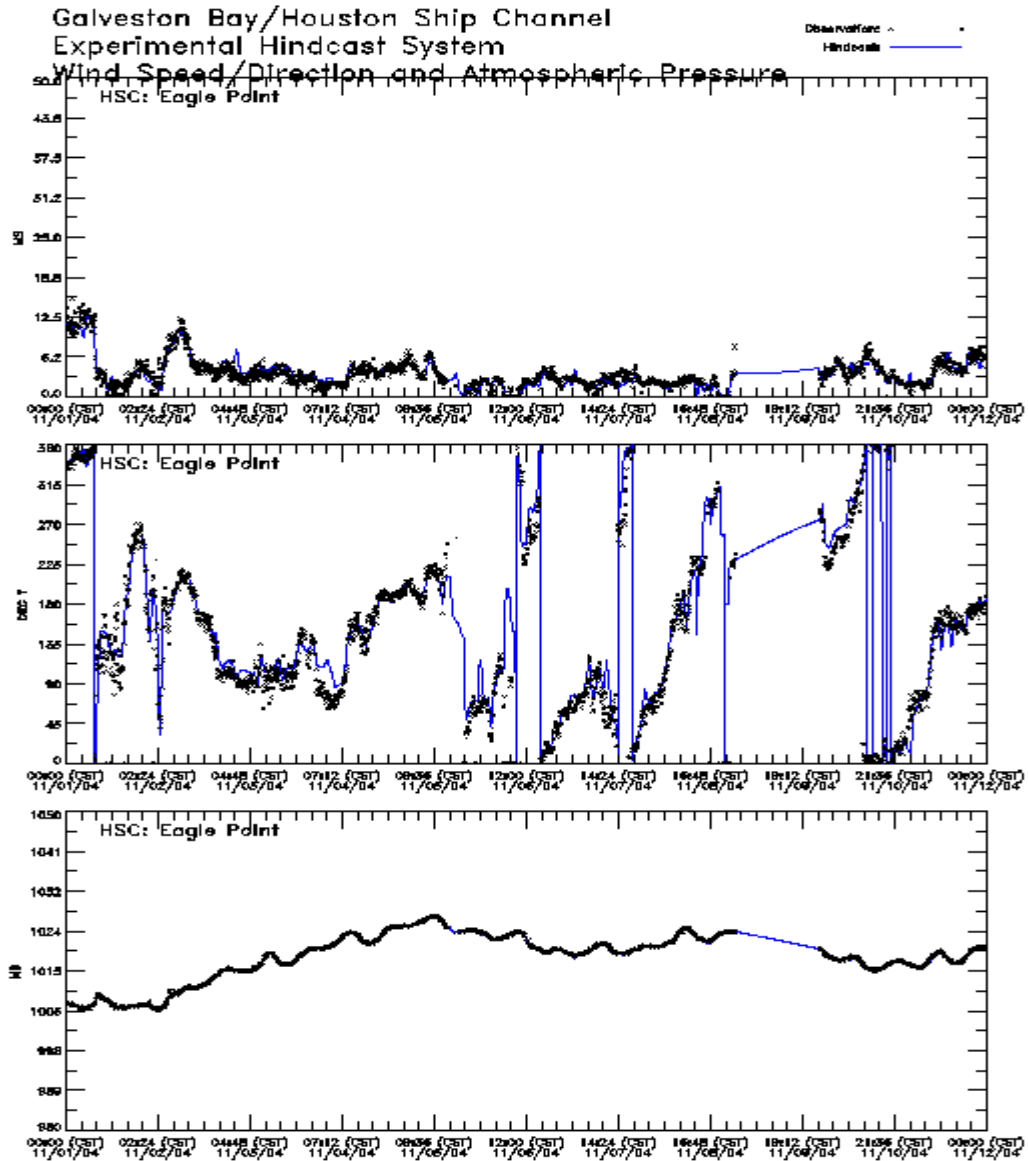
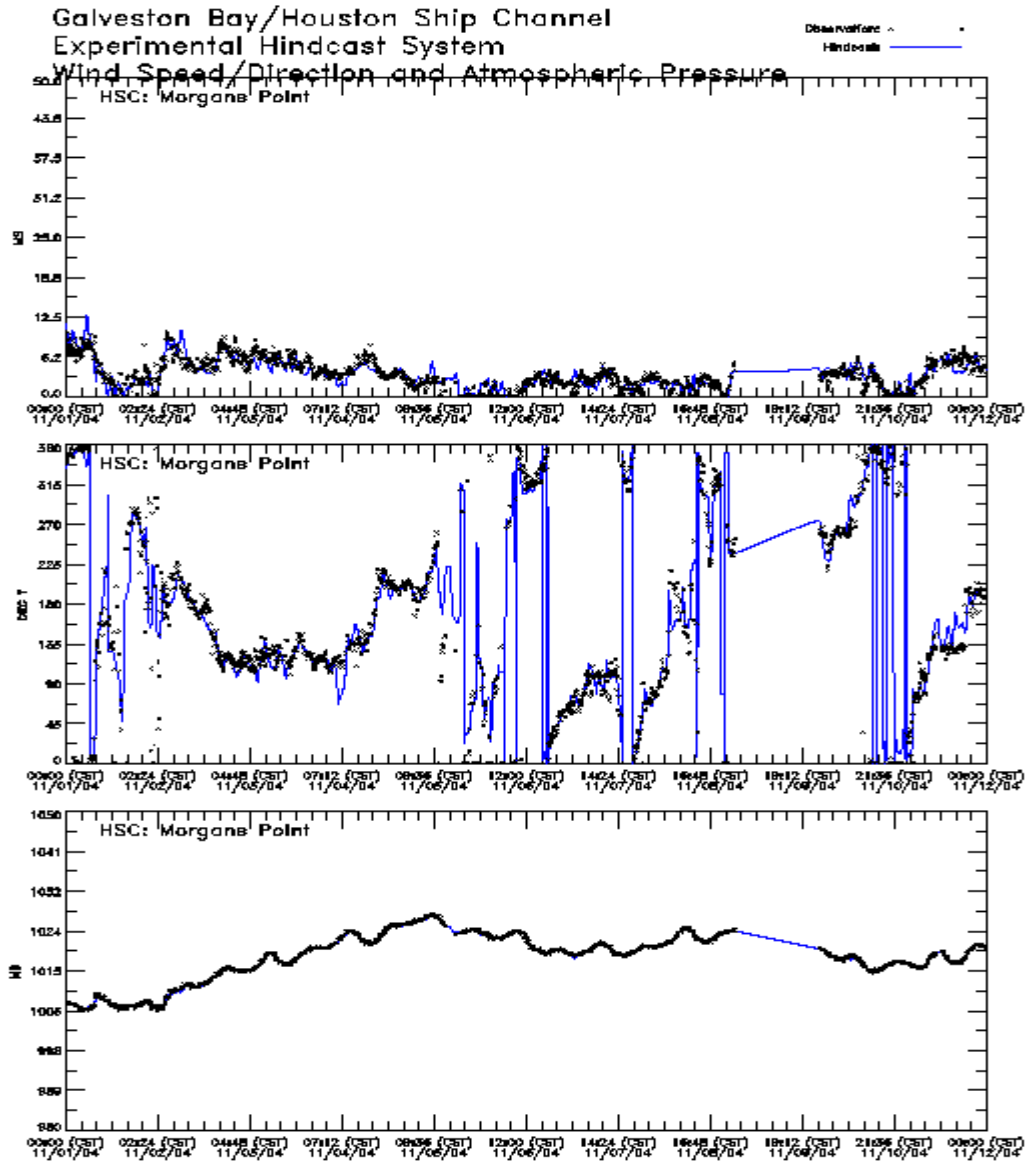


Figure 5.3. GBM winds and sea level atmospheric pressure at Bolivar Roads, November 1-12, 2004.



[Disclaimer: This product is under evaluation and should not be used for official purposes.]

Figure 5.4. HSCM winds and sea level atmospheric pressure at Eagle Point, November 1-12, 2004.



[Disclaimer: This product is under evaluation and should not be used for official purposes.]

Figure 5.5. HSCM winds and sea level atmospheric pressure at Morgans Point, November 1-12, 2004.

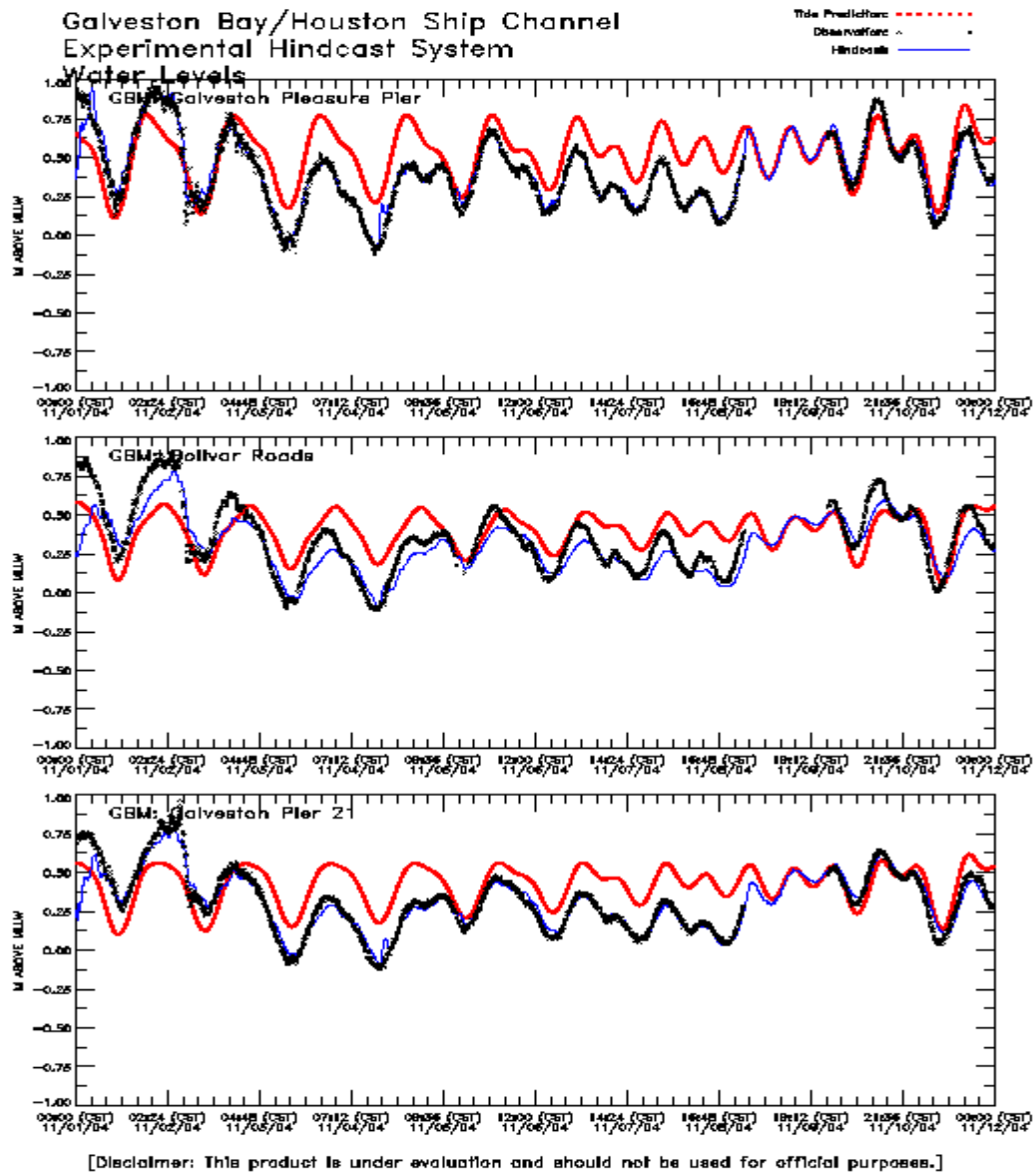
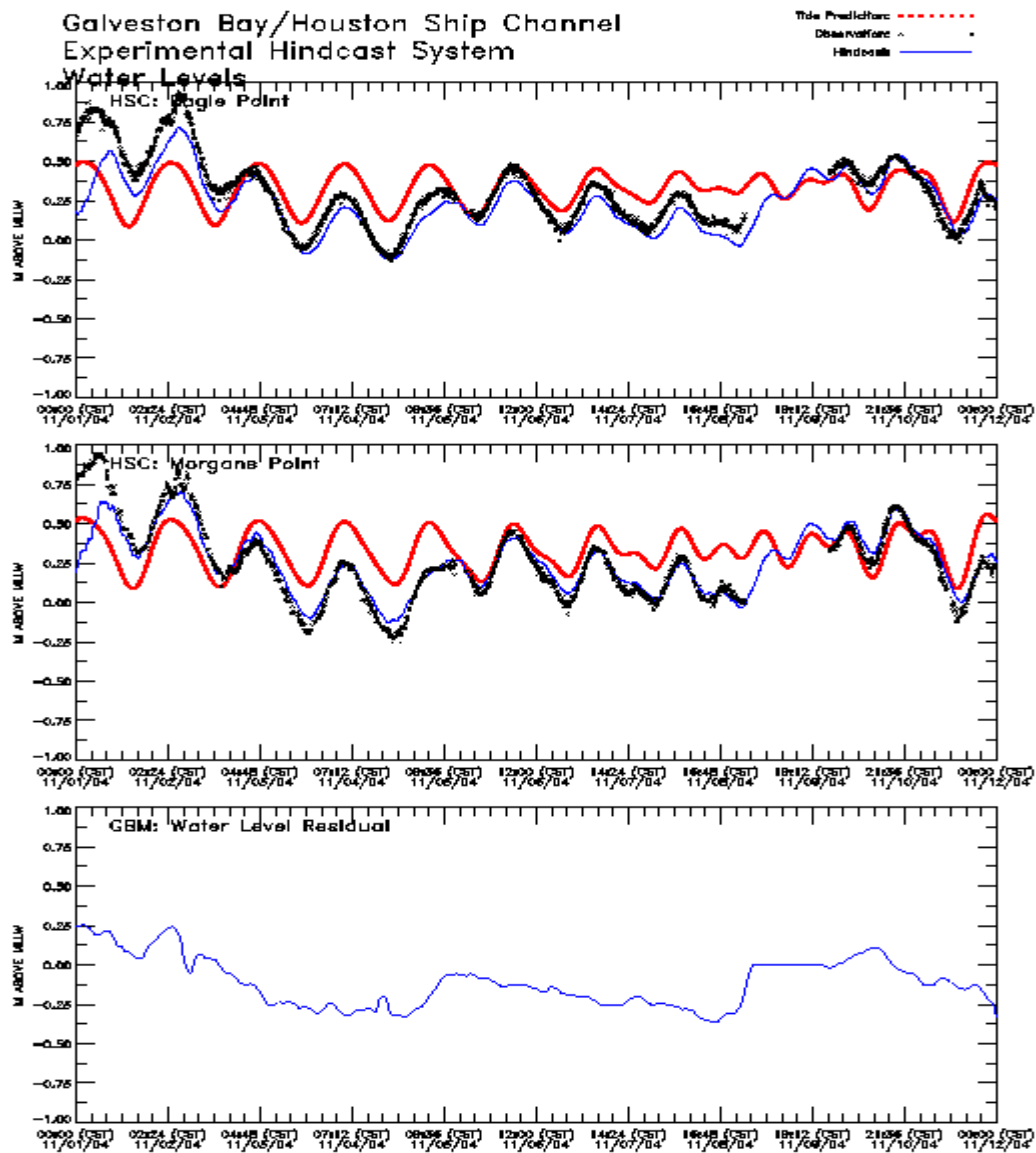


Figure 5.6. GBM simulated and observed water surface elevations at Galveston Pleasure Pier, Bolivar Roads, and Galveston Pier 21, November 1-12, 2004.



[Disclaimer: This product is under evaluation and should not be used for official purposes.]

Figure 5.7. HSCM simulated and observed water surface elevations at Eagle Point and Morgans Point and observed GBM water level residuals, November 1-12, 2004.

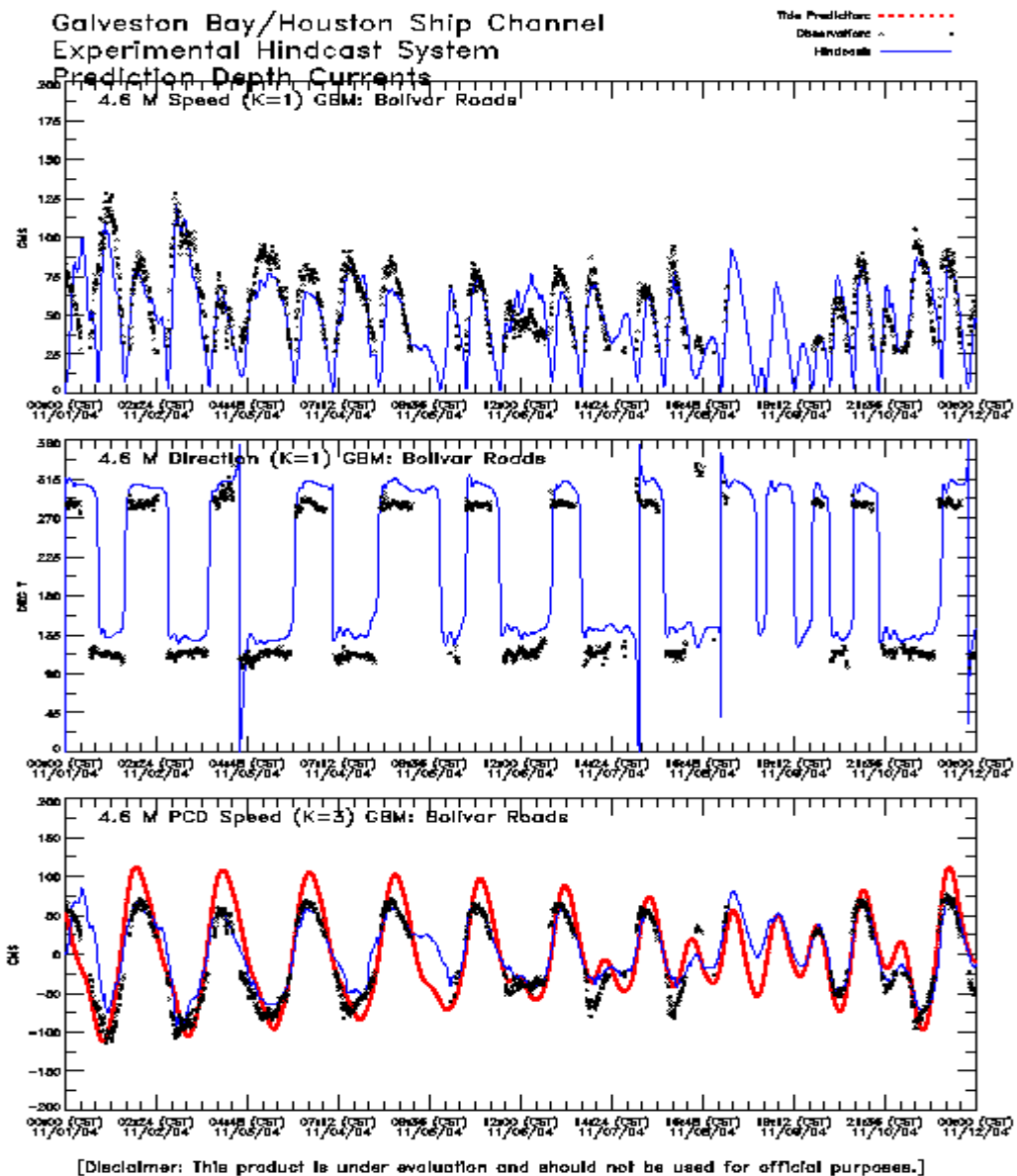


Figure 5.8. GBM simulated and observed prediction depth currents at Bolivar Roads, November 1-12, 2004.

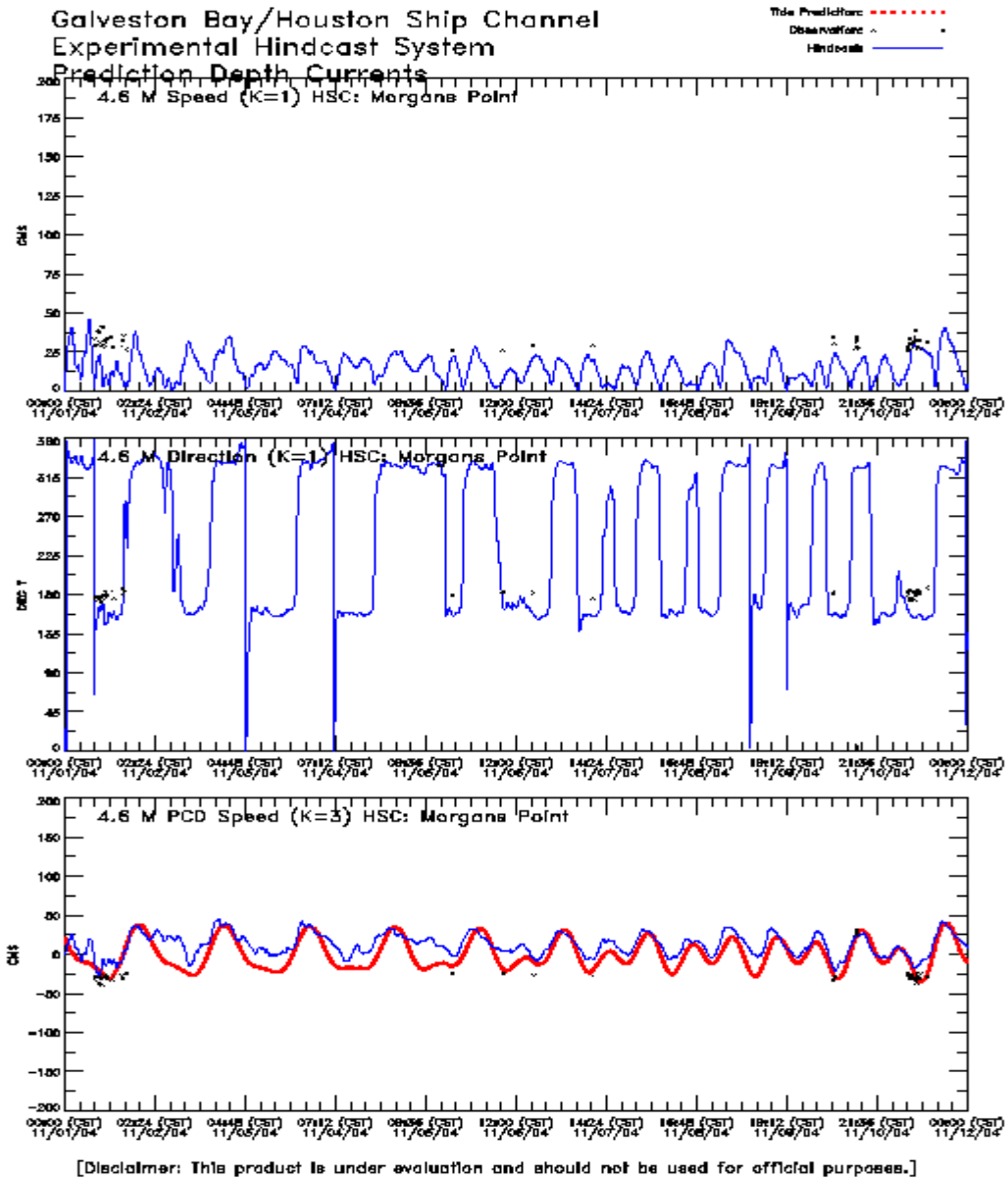


Figure 5.9. HSCM simulated and observed prediction depth currents at Morgans Point, November 1-12, 2004.

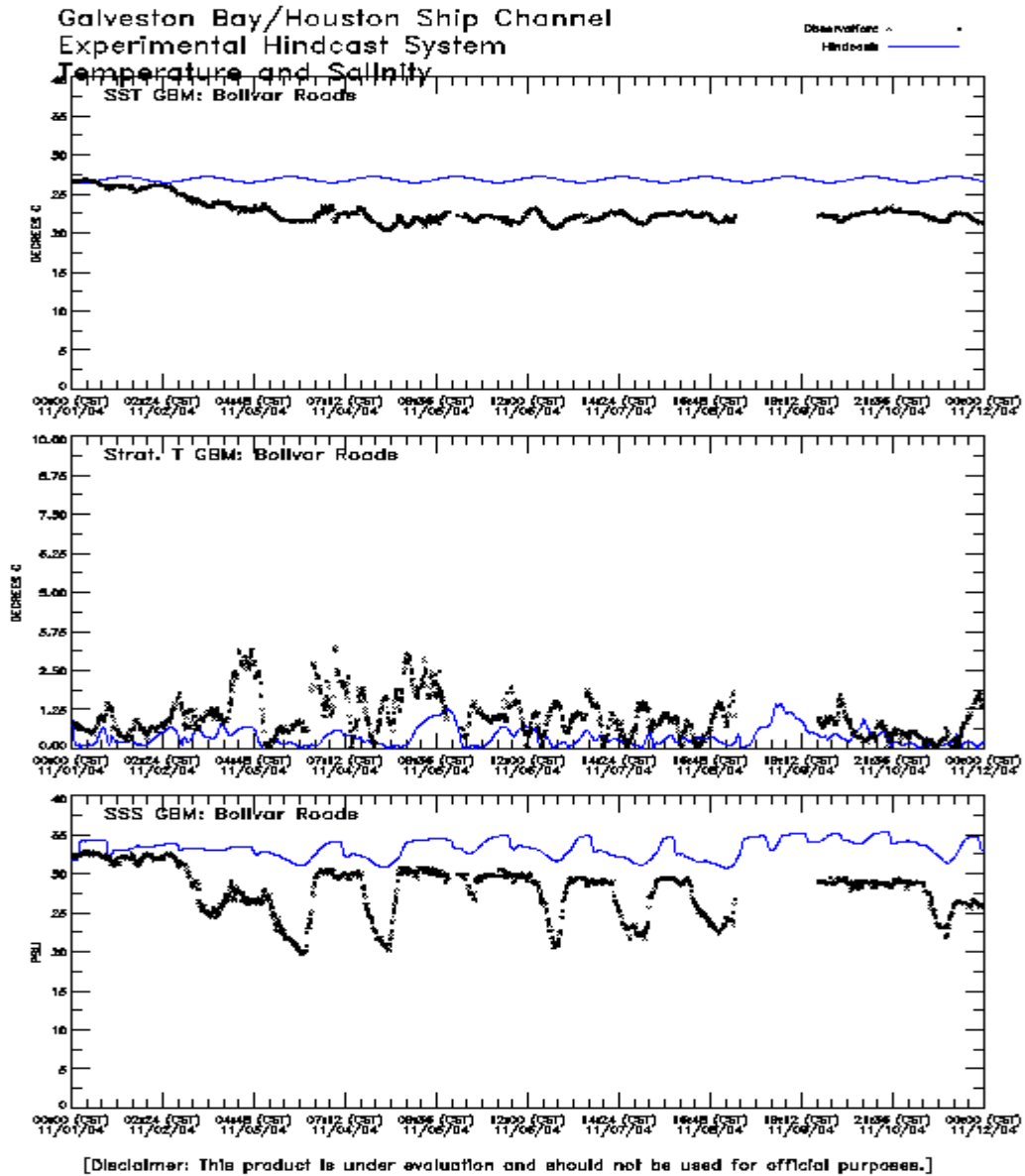


Figure 5.10. GBM simulated and observed temperature and surface salinity at Bolivar Roads, November 1-12, 20004.

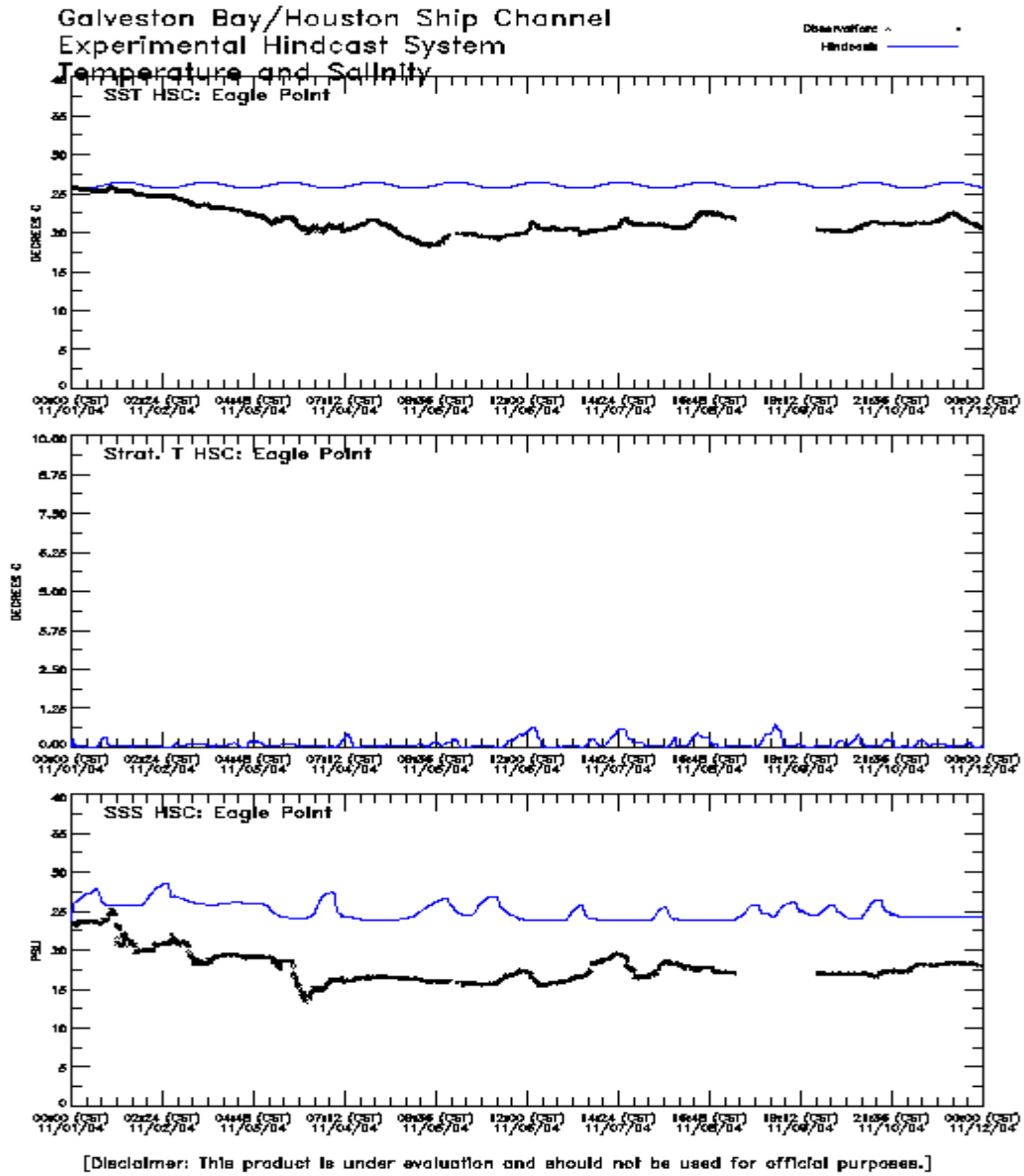


Figure 5.11. HSCM simulated and observed temperature and surface salinity at Eagle Point, November 1-12, 2004.

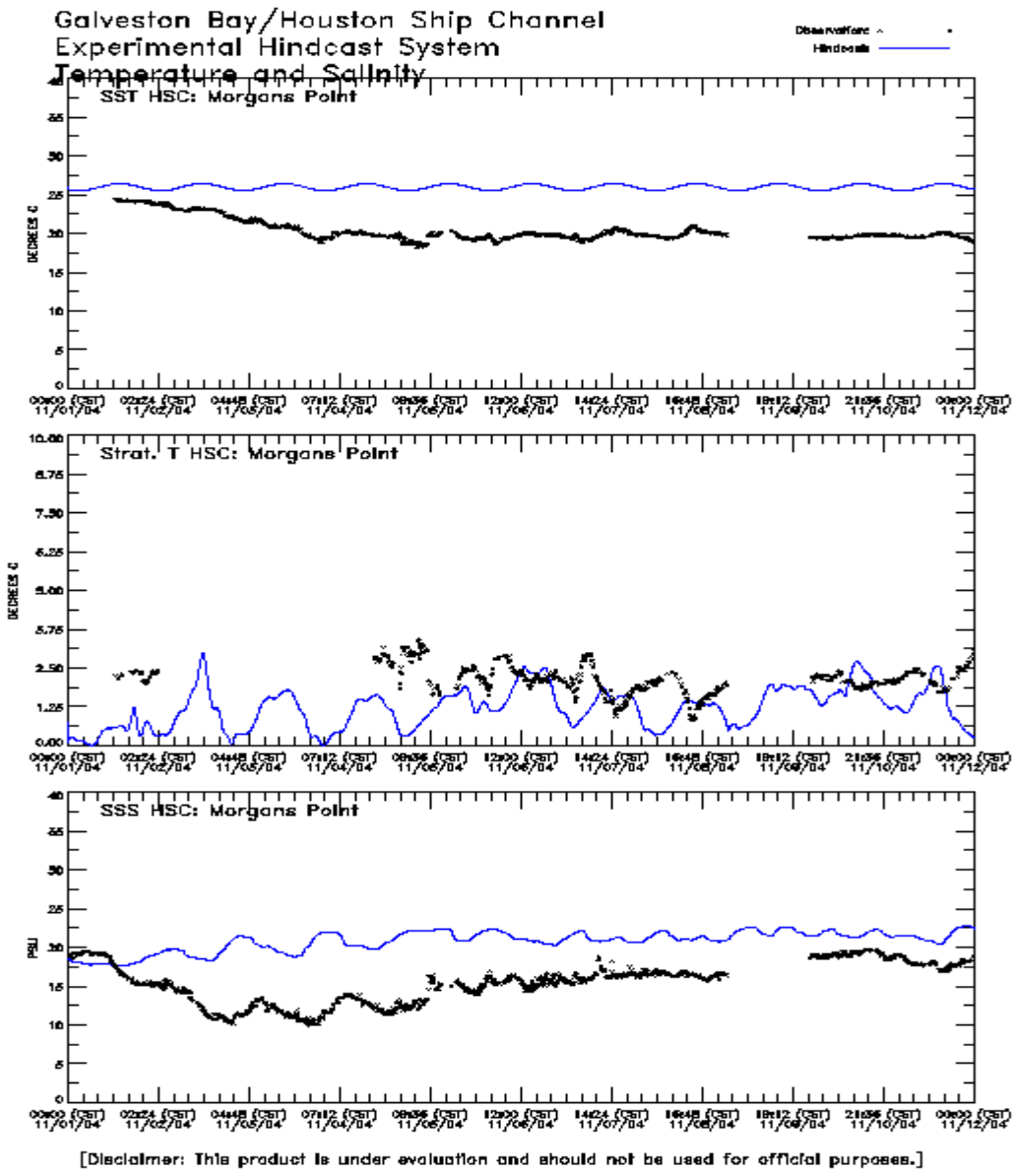


Figure 5.12. HSCM simulated and observed temperature and surface salinity at Morgans Point, November 1-12, 2004.

5.3. Short Wave Results

5.3.1. Significant Wave Height

Significant wave heights from the Galveston Bay model shown for 1 November 2004 in the top panel of Figure 5.13 are order 0.9m in the near shelf regions and are reduced to order 0.5m in the lower and upper Galveston Bay and West Bay regions. In the East Bay and Trinity Bay wave heights are order 0.3m. In the lower panel of Figure 5.13 significant wave heights from the Houston Ship Channel model agree in magnitude with those of the Bay model.

Significant wave heights from the Galveston Bay model shown for 12 November 2004 in the top panel Figure 5.14 are less than 0.5m throughout all Bay regions and on the near shelf. In the lower panel of Figure 5.14 significant wave heights from the Houston Ship Channel model agree in magnitude with those of the Bay model.

5.3.2. Wave Direction

Wave directions from the Galveston Bay model shown for 1 November 2004 in the top panel of Figure 5.15 are to the North consistent with the wind directions shown in Figures 5.3-5.5. Wave directions are equal to the wind directions as obtained from a two-step Barnes interpolation from the PORTS stations. The Barnes interpolation procedure does not guarantee strict equality of the interpolated and injected data point. Wave directions from the Houston Ship Channel model in the lower panel of Figure 5.15 are in general agreement with those of the Bay model, but may be slightly different due to the fact that a separate Barnes interpolation is performed over the Channel model domain.

Wave directions from the Galveston Bay model shown for 12 November 2004 in the top panel of Figure 5.16 are from the North consistent with the wind directions shown in Figures 5.3-5.5. Again the same remarks regarding the two-step Barnes interpolation from the PORTS stations apply. Wave directions from the Houston Ship Channel model in the lower panel of Figure 5.16 are in general agreement with those of the Bay model, but may be slightly different due to the separate Barnes interpolation.

5.3.3. Wave Period

Wave periods from the Galveston Bay model shown for 1 November 2004 in the top panel of Figure 5.17 are order 3-4 sec, with 5 sec waves found in the near shelf regions and in the deeper navigation channel. In the lower panel of Figure 5.17 wave periods from the Houston Ship Channel model agree in magnitude with those of the Bay model with longer period waves being again found in the navigation channel.

Wave periods from the Galveston Bay model shown for 12 November 2004 in the top panel Figure 5.18 are of the same order as found on 1 November. In the lower panel of Figure 5.18 wave periods from the Houston Ship Channel model agree in magnitude with those of the Bay model.

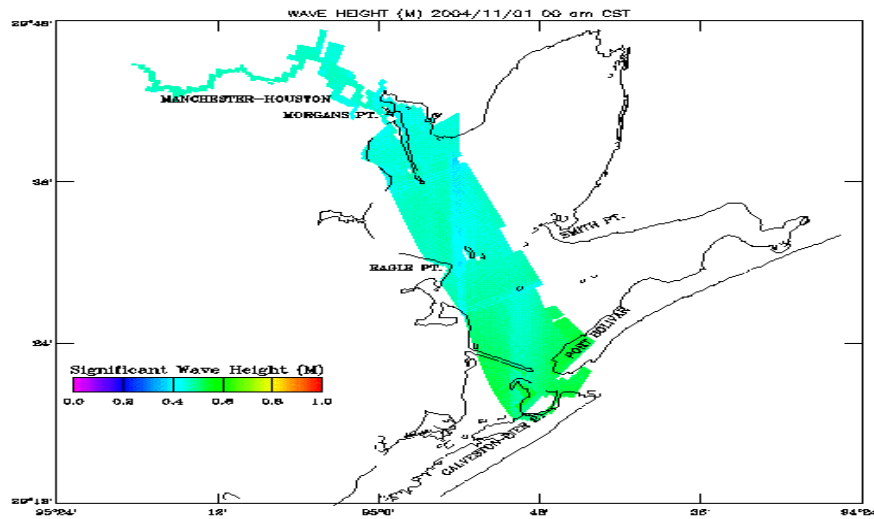
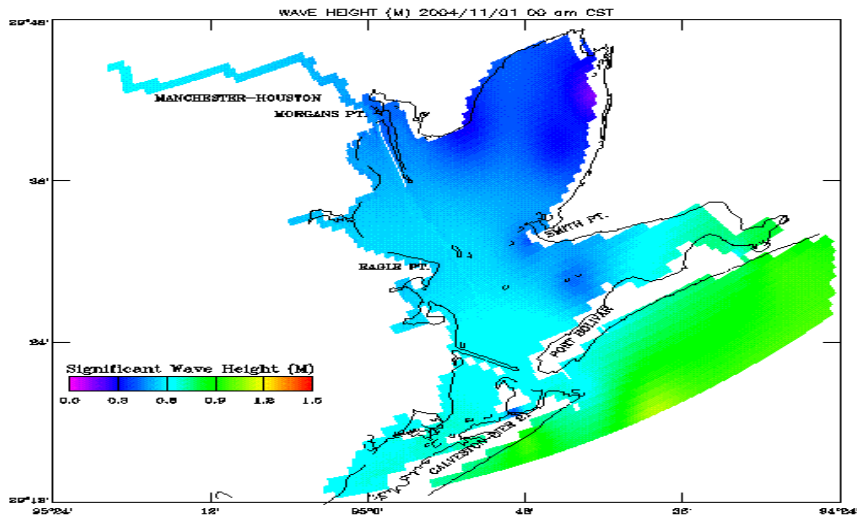


Figure 5.13. GBM and HSCM simulated significant wave height, November 1, 2004.

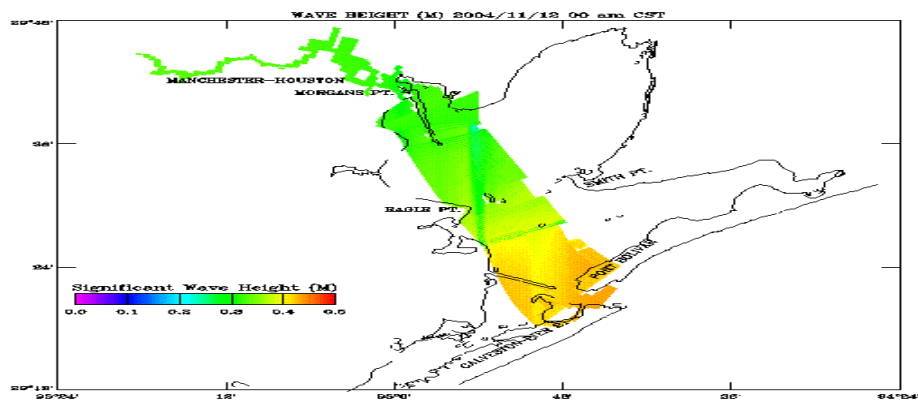
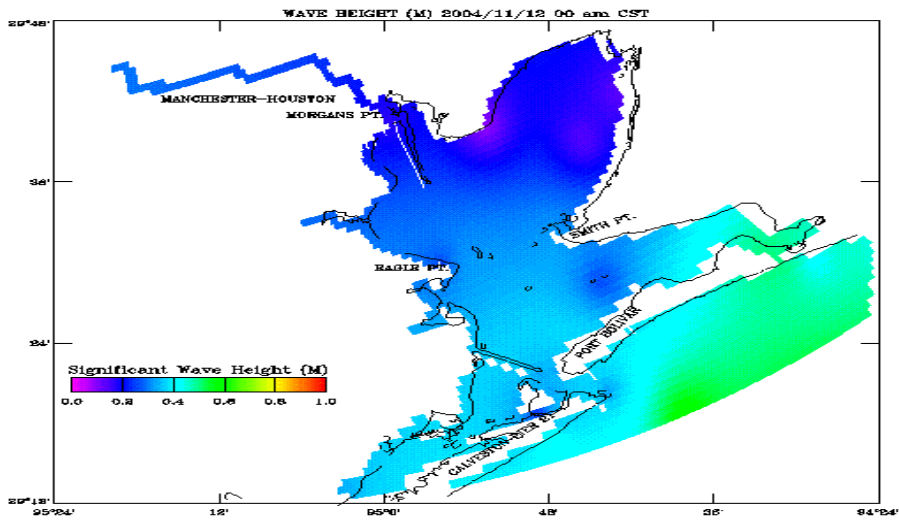


Figure 5.14. GBM and HSCM simulated significant wave height, November 12, 2004

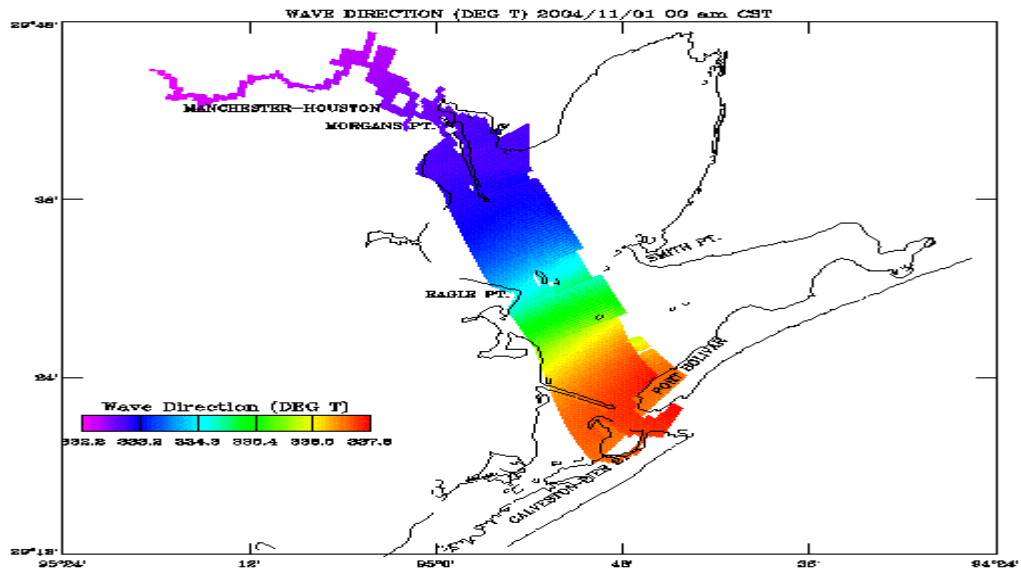
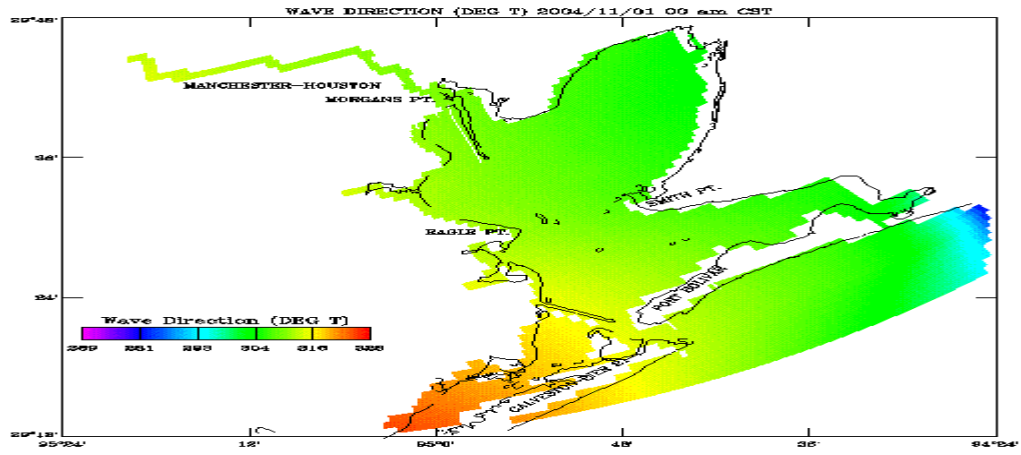


Figure 5.15. GBM and HSCM simulated wave direction, November 1, 2004.

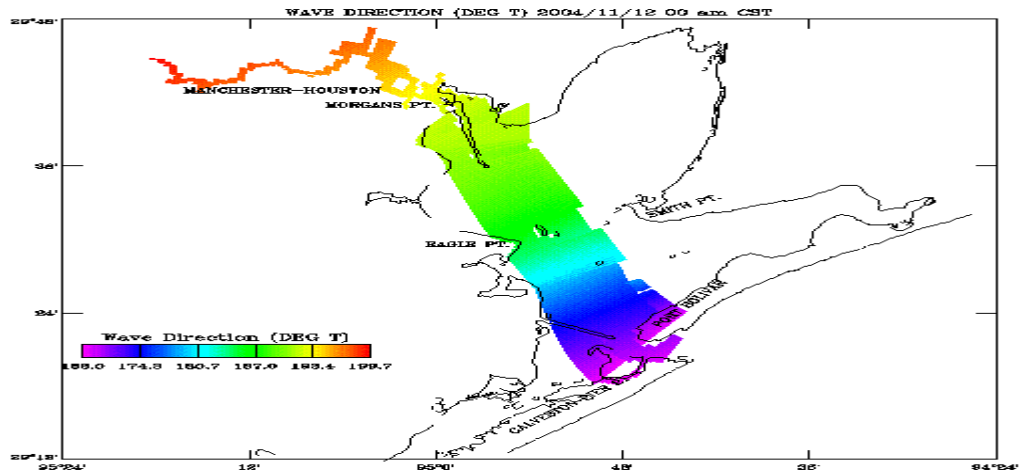
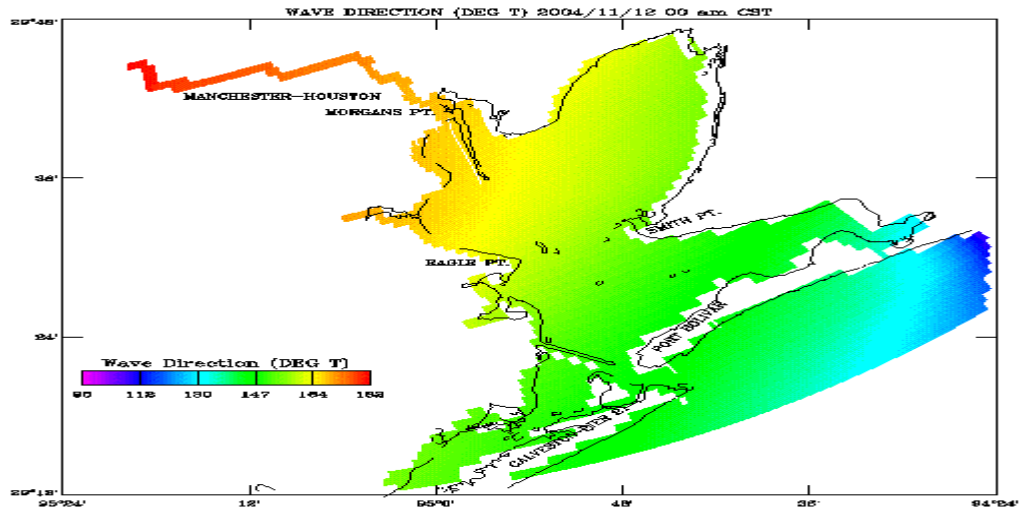


Figure 5.16. GBM and HSCM simulated wave direction, November 12, 2004.

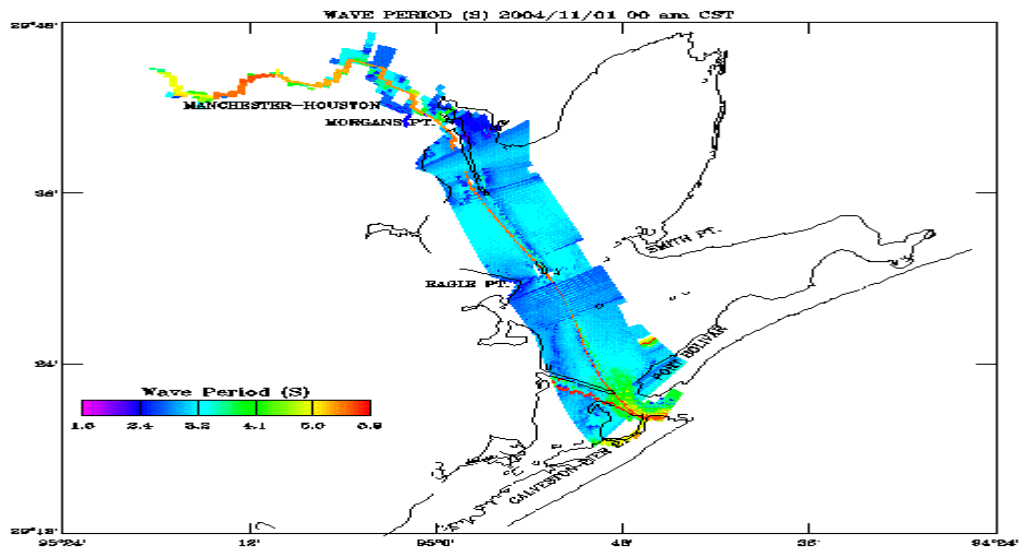
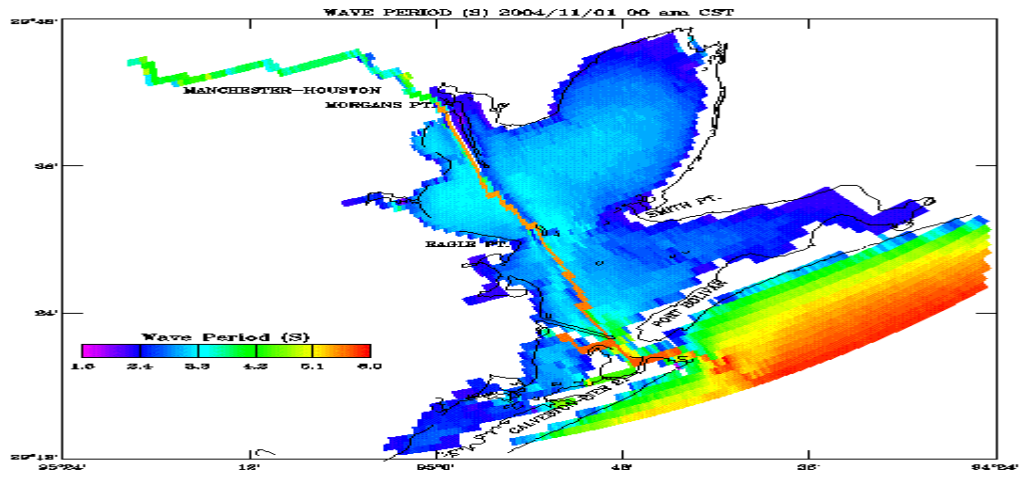


Figure 5.17. GBM and HSCM simulated wave period, November 1, 2004.

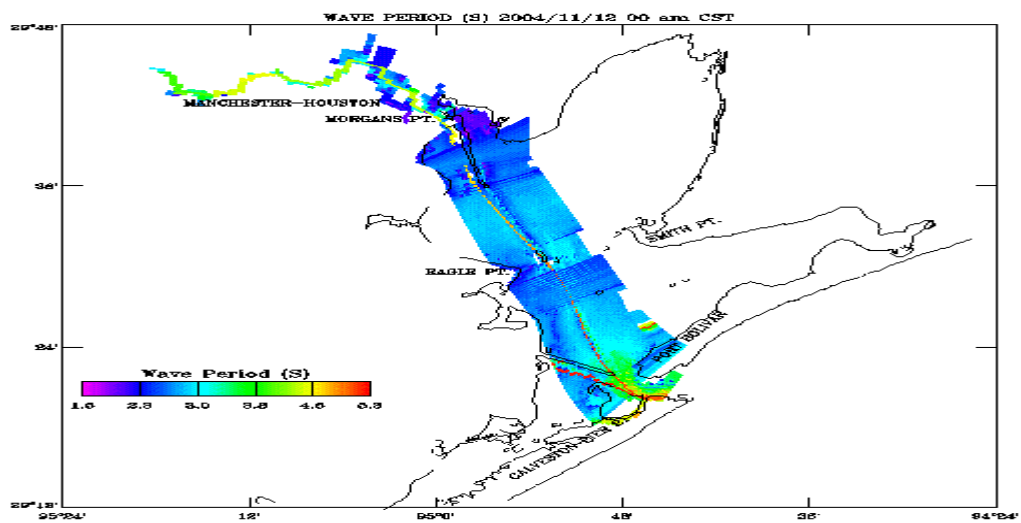
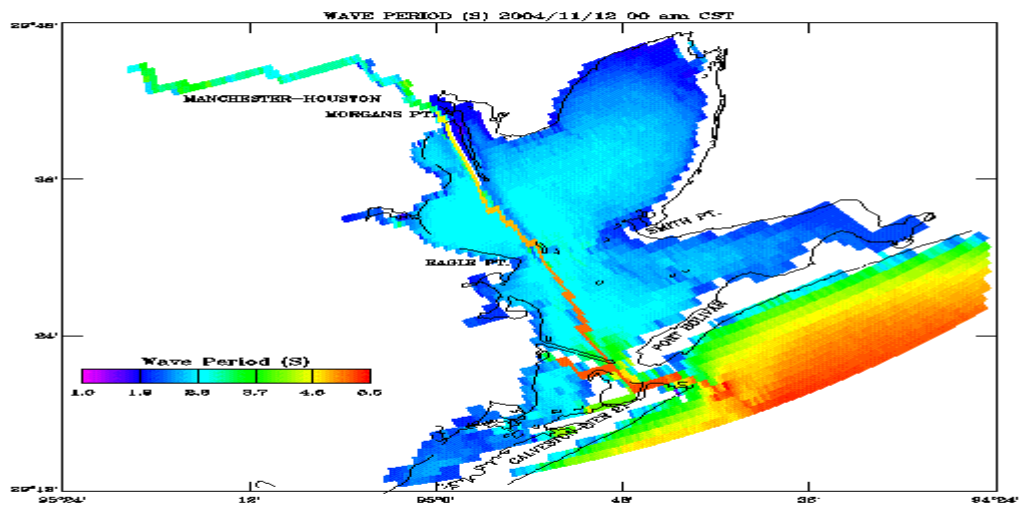


Figure 5.18. GBM and HSCM simulated wave period, November 12, 2004.

5.4. SF₆ Tracer Results

5.4.1. Concentration Fields

Near surface Galveston Bay Model SF₆ concentration fields 10 days after the injection, on 00 CST on 12 November, 2004 are shown in Figure 5.19. In the top panel, results are shown for the case of surface gas transfer, while in the bottom panel results are shown for no surface gas transfer. For the no surface flux case, the surface concentrations are elevated from those for the surface flux case and present in the lower portions of the Port of Houston at Morgans Point.

Near bottom Galveston Bay Model SF₆ concentration fields are given in Figure 5.20. In the top panel, results are shown for the case of surface gas transfer, while in the bottom panel results are shown for no surface gas transfer. Note that in the surface flux CS1 fields, the maximum legend value is order 10³ and the concentrations are elevated at the bottom (from the surface, Figure 5.19 top panel). In the no surface flux CS2 fields, the maximum legend value is 10⁴ and the fields are uniformly mixed over the vertical.

Corresponding results for the Houston Ship Channel Model SF₆ concentration fields are shown at the near surface in Figure 5.21 and at the near bottom in Figure 5.22. The SF₆ tracer reaches the boundary and therefore there is some uncertainty as to the influence of the zero flux inflow condition on the results. The southern extent of the tracer in both surface and bottom figures is reduced from the Bay model results.

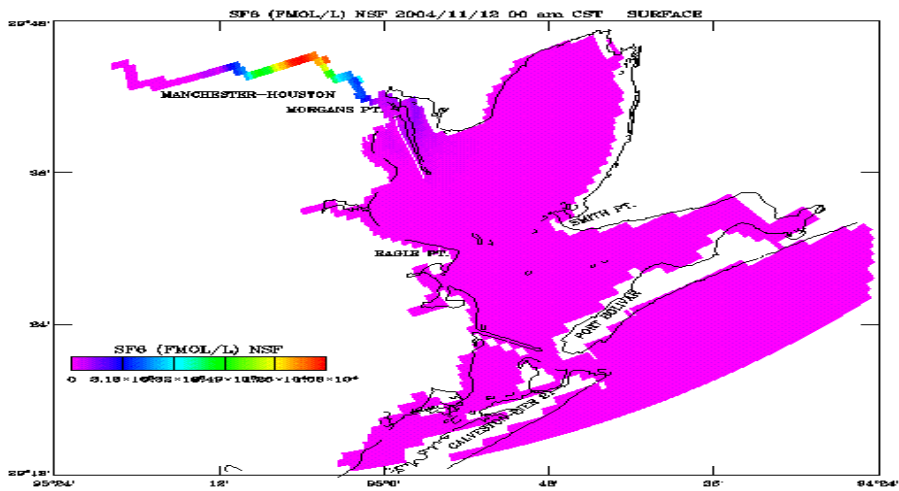
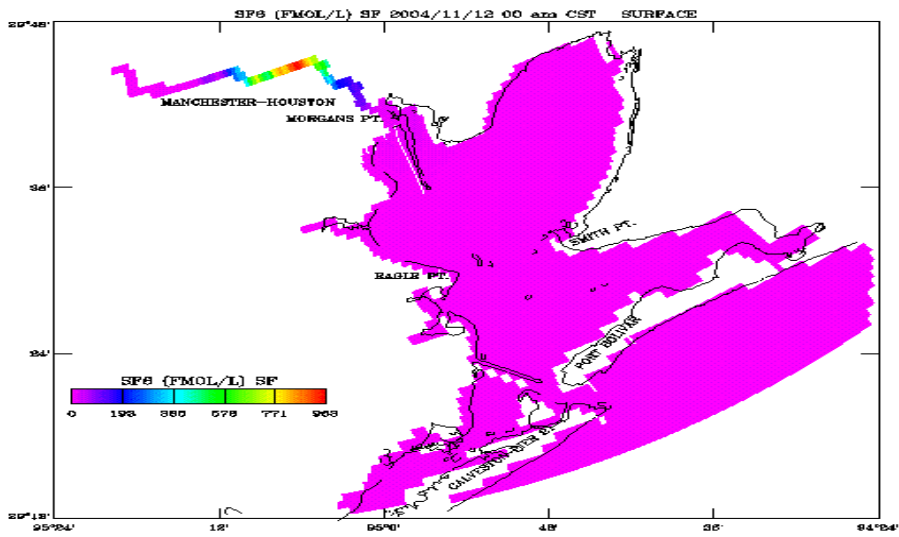


Figure 5.19. GBM simulated near surface SF₆ Concentrations at 00 CST on 12 November, 2004. (Upper panel surface flux (CS1), Lower panel no surface flux (CS2)).

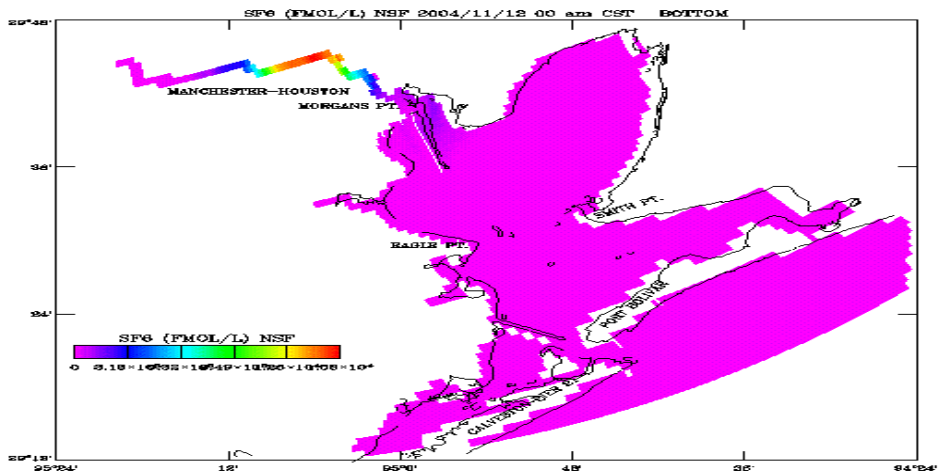
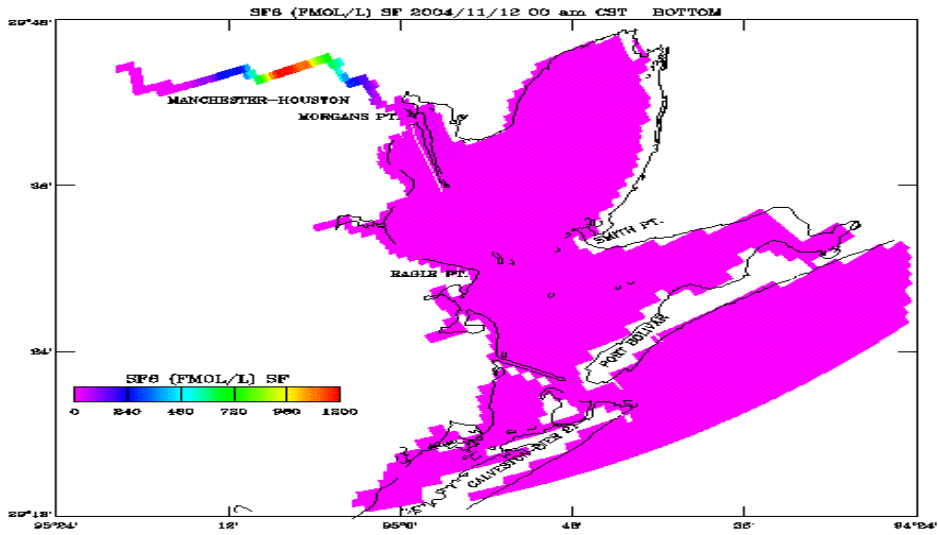


Figure 5.20. GBM simulated near bottom SF₆ Concentrations at 00 CST on 12 November, 2004. (Upper panel surface flux (CS1), Lower panel no surface flux (CS2)).

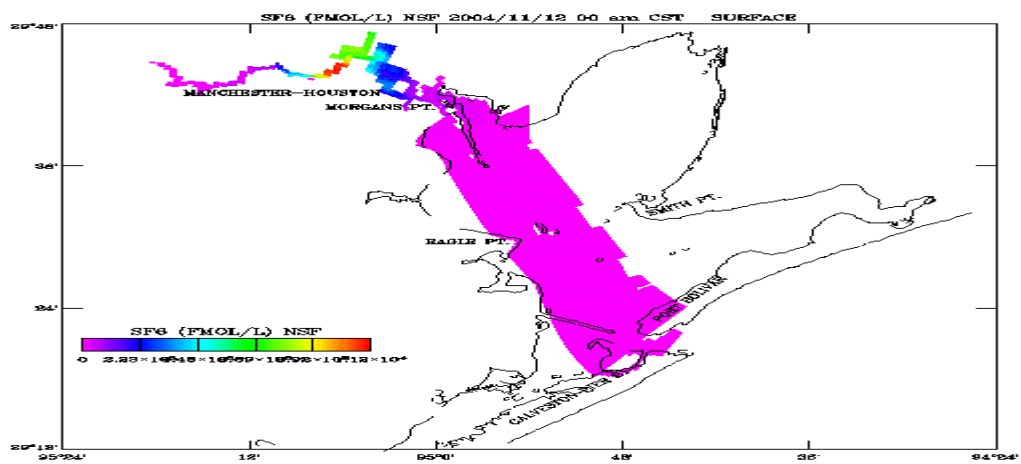
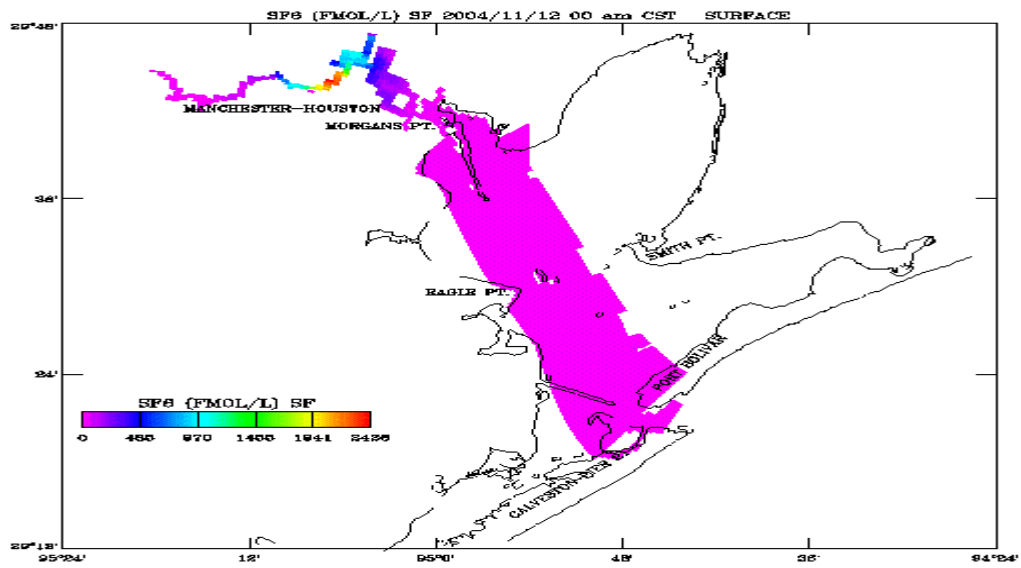


Figure 5.21. HSCM simulated near surface SF₆ Concentrations at 00 CST on 12 November, 2004. (Upper panel surface flux (CS1), Lower panel no surface flux (CS2)).

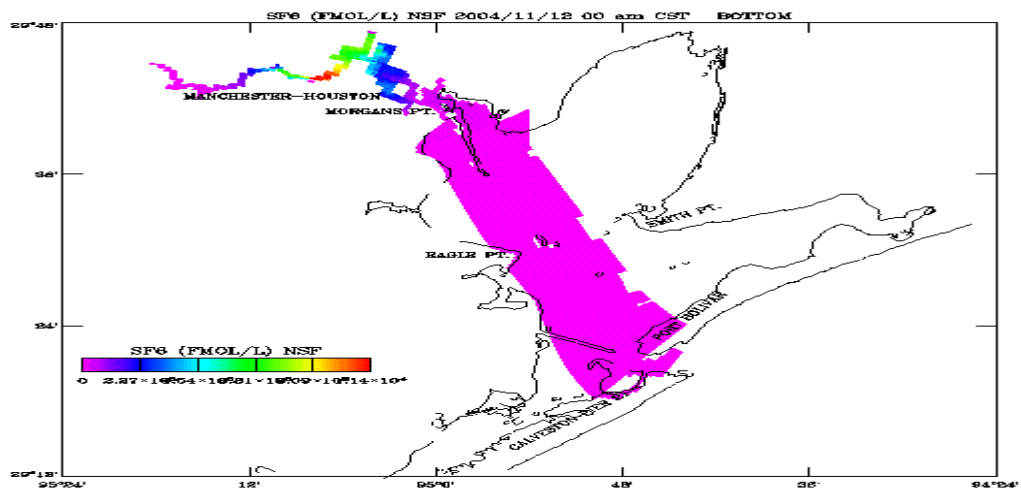
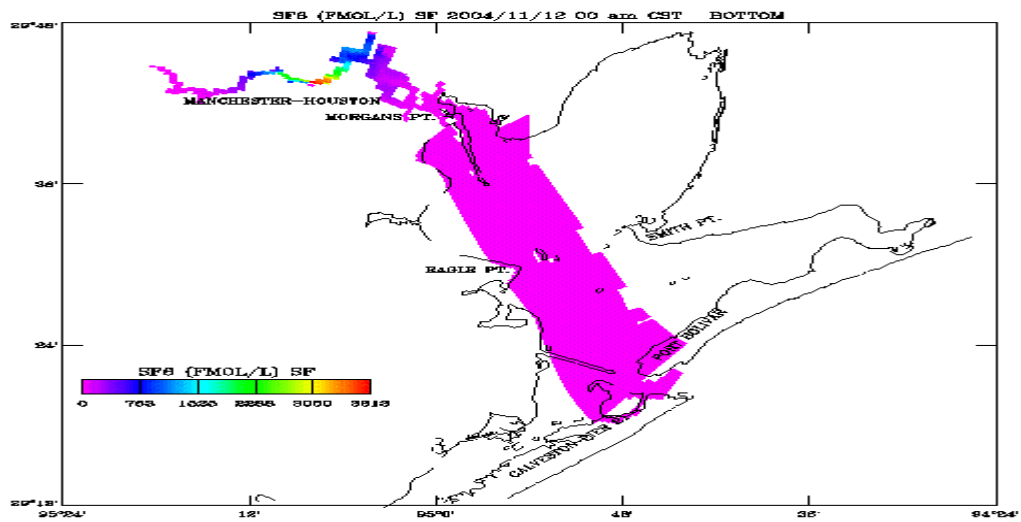


Figure 5.22. HSCM simulated near bottom SF₆ Concentrations at 00 CST on 12 November, 2004. (Upper panel surface flux (CS1), Lower panel no surface flux (CS2)).

5.4.2. Residence Time

The time to exposure for SF₆ is defined as the time since the start of the injection when the concentration at the given point exceeded a threshold value of 2 fmol/L. The residence time is defined as the difference in the time to exposure of the given point and the injection point. Since at the injection time, the initial concentration of SF₆ equaled 457937 fmol/L in all 5 vertical levels in the GBM and equaled 515151 fmol/L in all 5 vertical levels in the HSCM, which exceeded the threshold value, the time to exposure and residence times are equivalent.

In Figure 5.23, the GBM near surface residence times are given for CS1 surface flux and CS2 no surface flux. In the case of no surface flux, the extent of the nonzero residence time is greatly enhanced. This may be used by the field research team to plan the area of coverage over a ten day experiment. In Figure 5.24, the GBM near bottom residence times are given for CS1 and CS2, with the areal coverage of nonzero residence time increased for the no surface flux condition. The area of nonzero residence time at the surface for CS1 is similar to the bottom area. For CS2 the surface and bottom areas are quite different.

In Figures 5.25 and 5.26, the corresponding HSCM residence time results are shown. Note that the southern extent of the nonzero residence times is reduced from that shown in the GBM. The extent of the nonzero residence time, however, does reach the lateral boundaries and this may be a source of error, since a zero gradient condition is used on inflow.

5.4.3. Exposure Level and Duration

To further assess the exposure, the average exposure level and maximum exposure levels are determined as well as the duration of the exposure. Note the exposure level is determined as the concentration of SF₆ exceeding the threshold value of 2 fmol/L. While these results are available at each of the 5 vertical layers, we examine here only the first near surface layer. The near surface average and maximum exposure levels are shown in Figure 5.27 and Figure 5.28, respectively, for both of the models. In Figure 5.29, the duration of exposure is presented. These type of computations should enable direct exposure assessments.

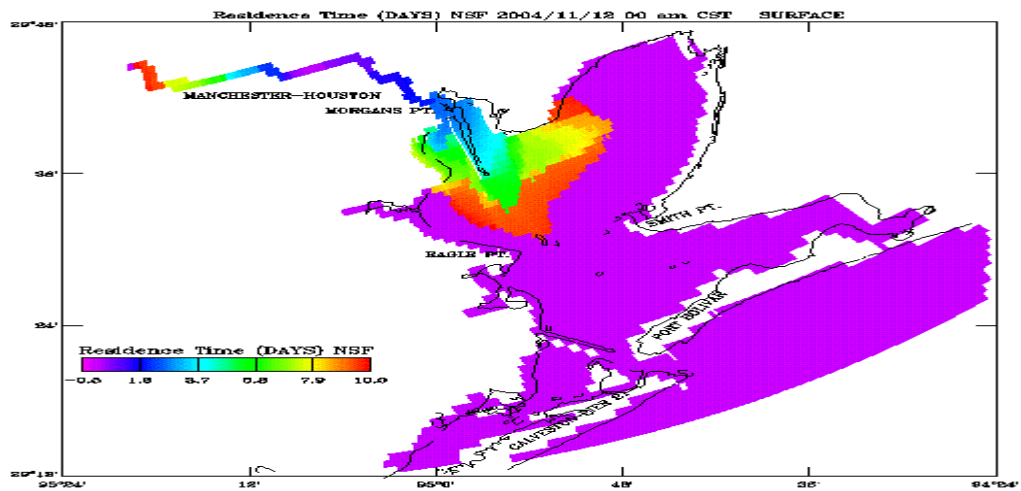
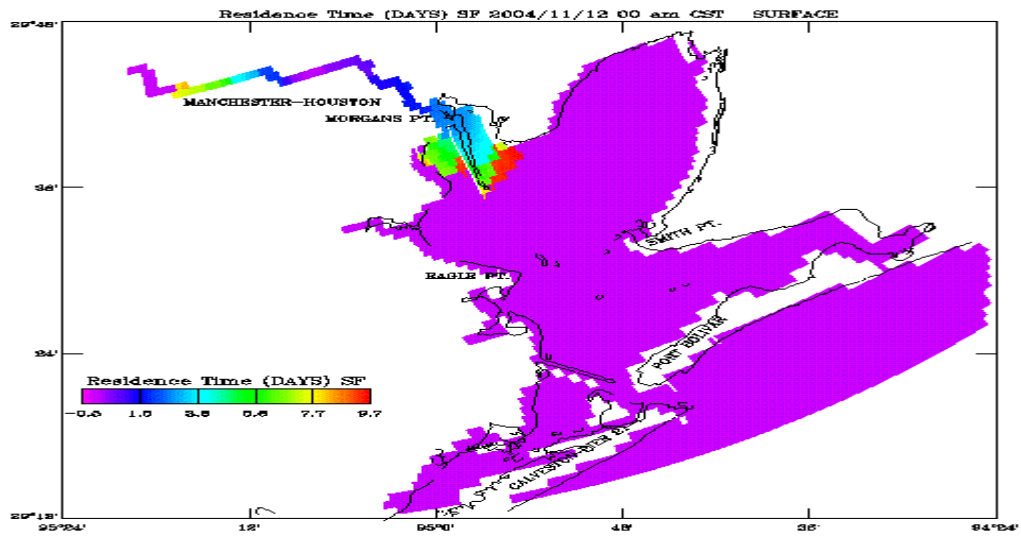


Figure 5.23. GBM near surface residence time. (Upper panel surface flux (CS1), Lower panel no surface flux (CS2)).

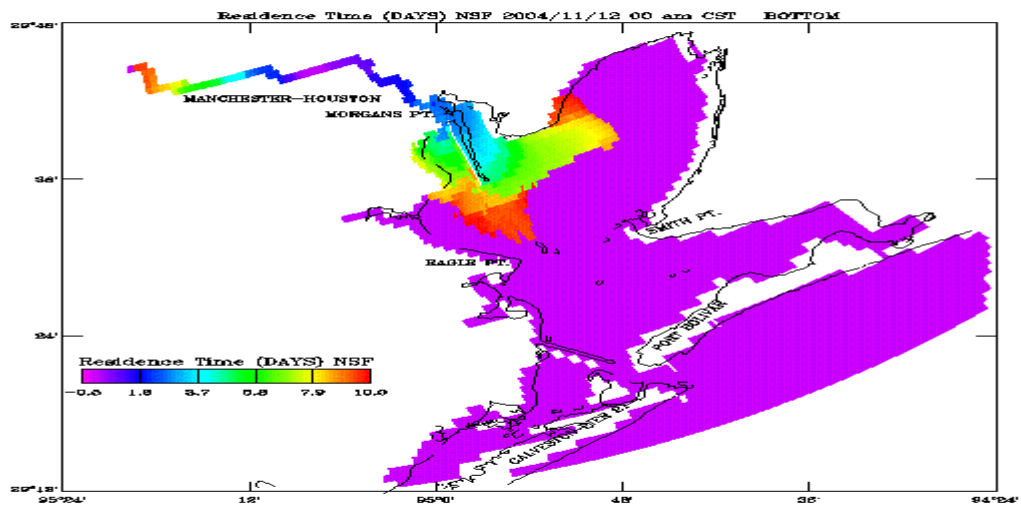
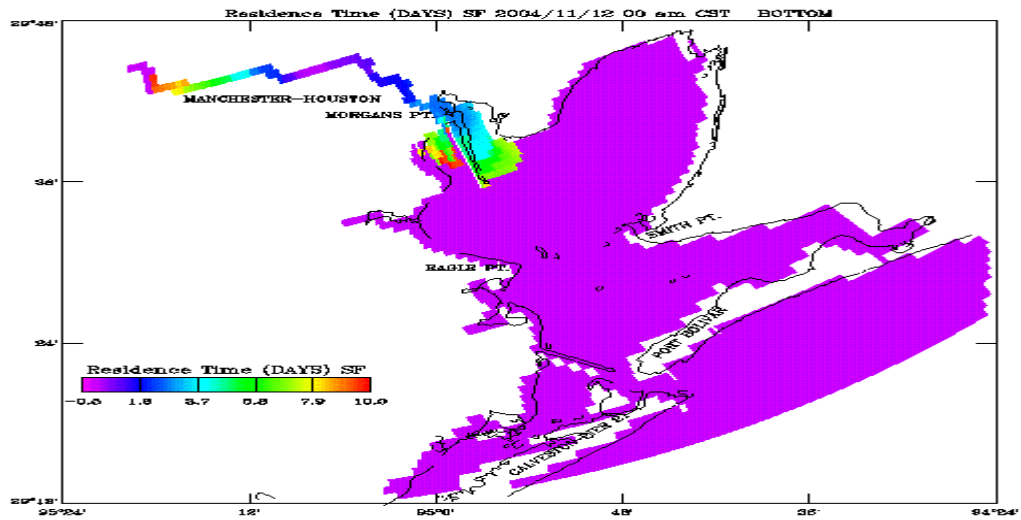


Figure 5.24. GBM simulated near bottom residence time. (Upper panel surface flux (CS1), Lower panel no surface flux (CS2)).

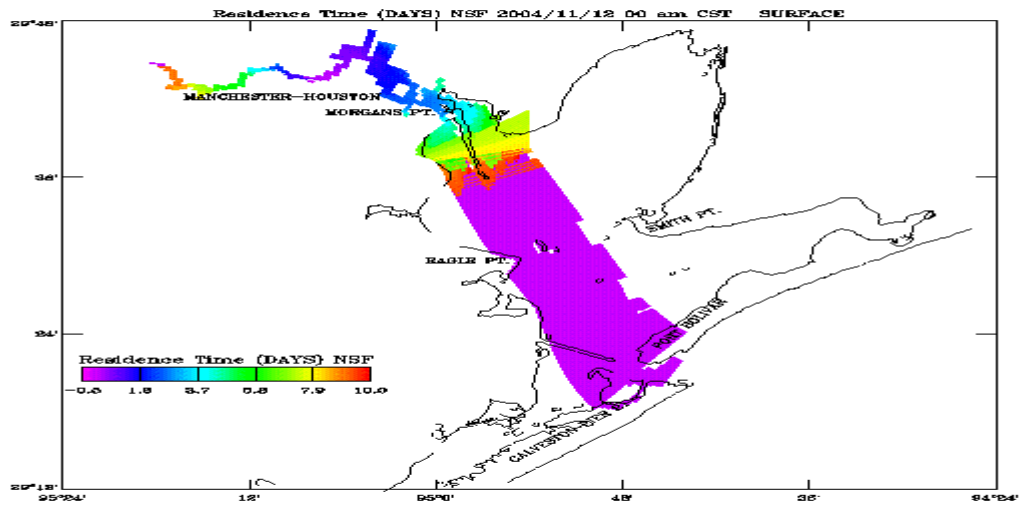
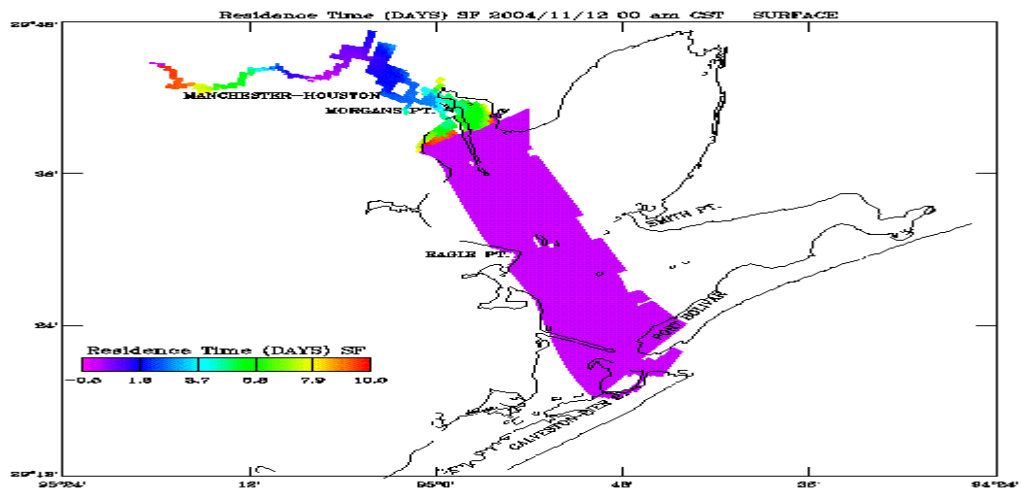


Figure 5.25. HSCM simulated near surface residence time. (Upper panel surface flux (CS1), Lower panel no surface flux (CS2)).

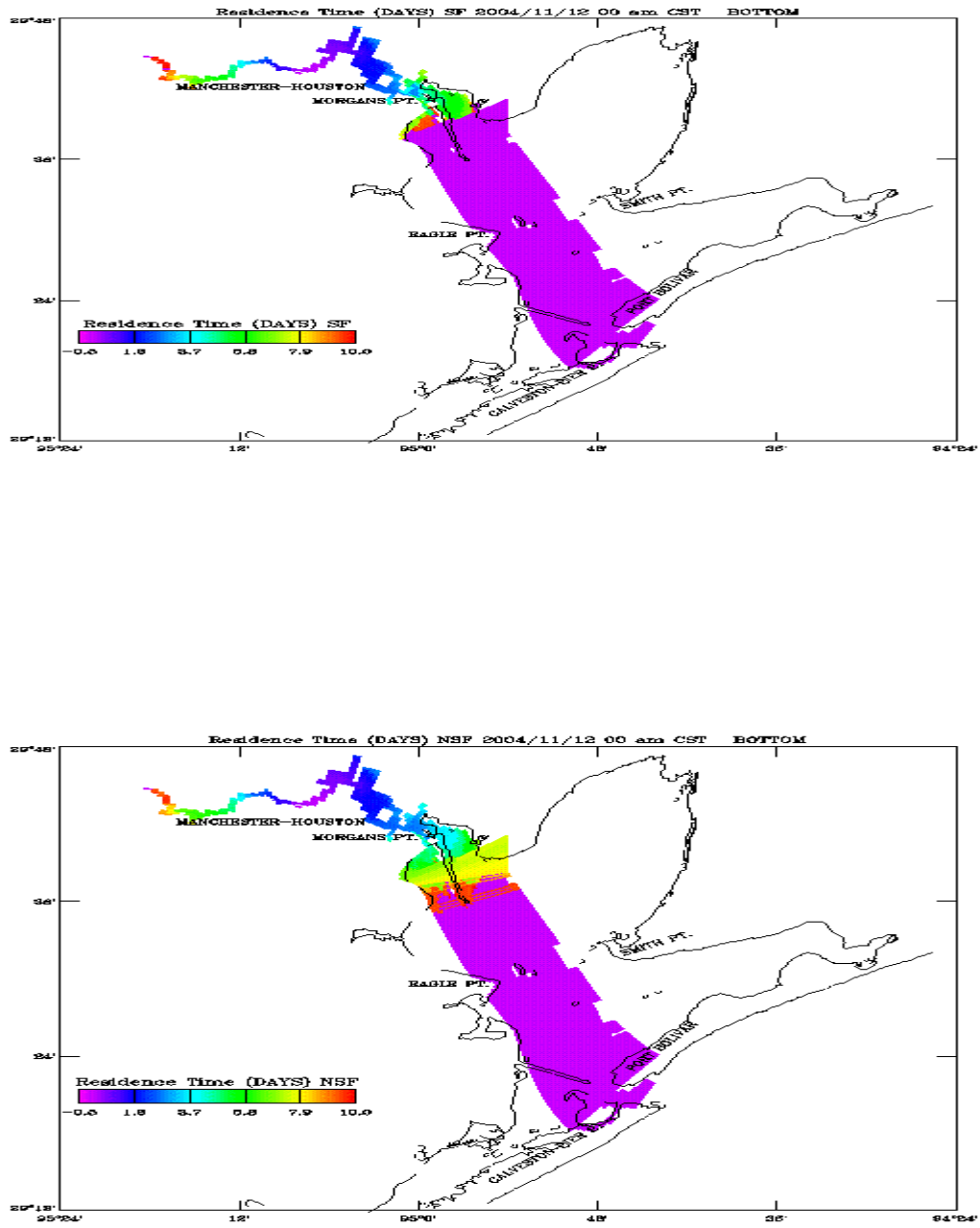


Figure 5.26. HSCM simulated near bottom residence time. (Upper panel surface flux (CS1), Lower panel no surface flux (CS2)).

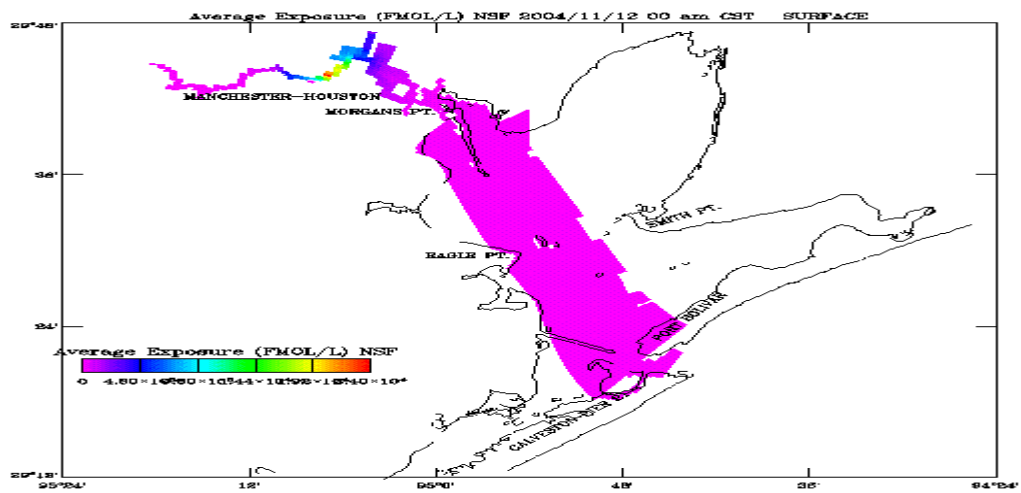
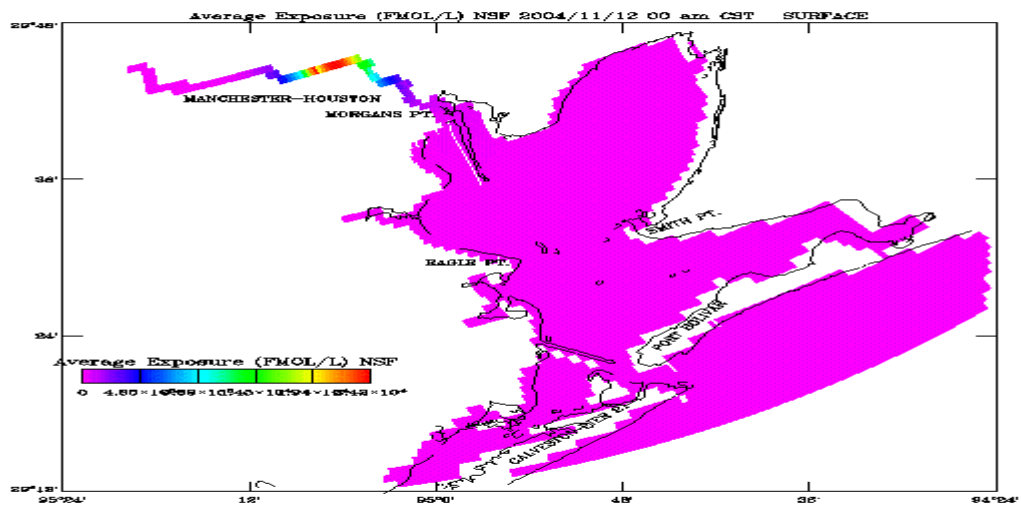


Figure 5.27. Simulated near surface no surface flux (CS2) average exposure levels (fMOL/L). (Upper panel GBM, Lower panel HSCM).

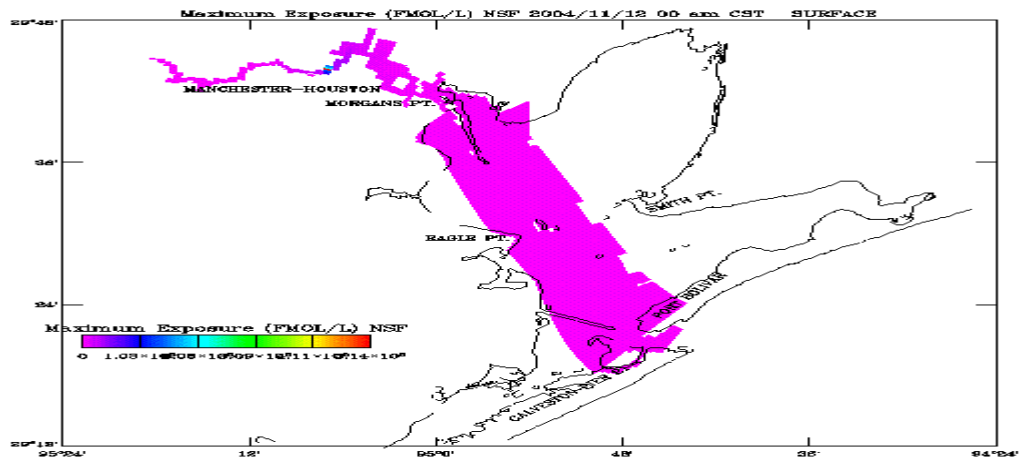
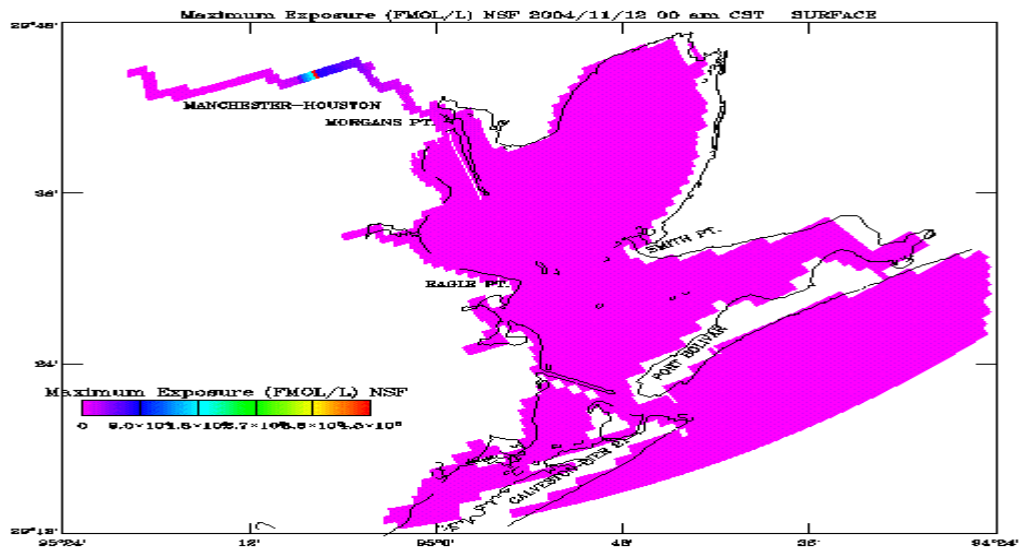


Figure 5.28. Simulated near surface no surface flux (CS₂) maximum exposure levels (fmol/L). (Upper panel GBM, Lower panel HSCM).

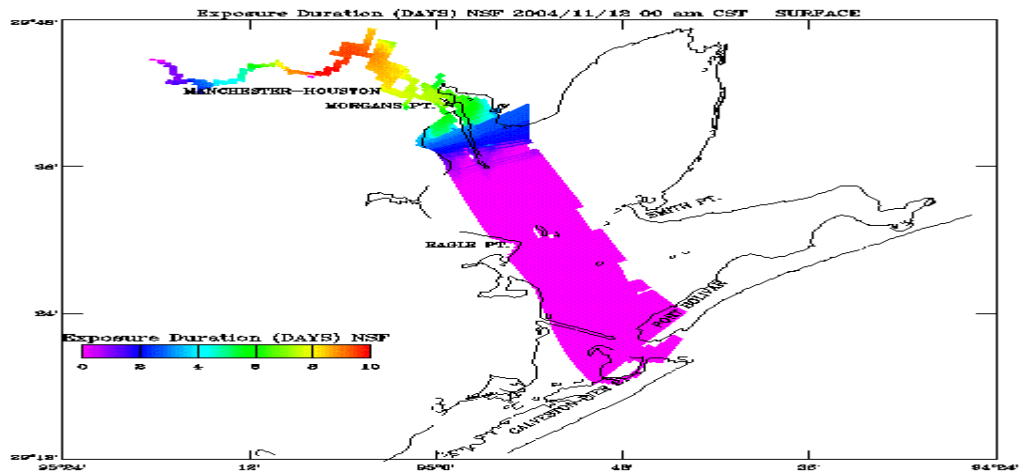
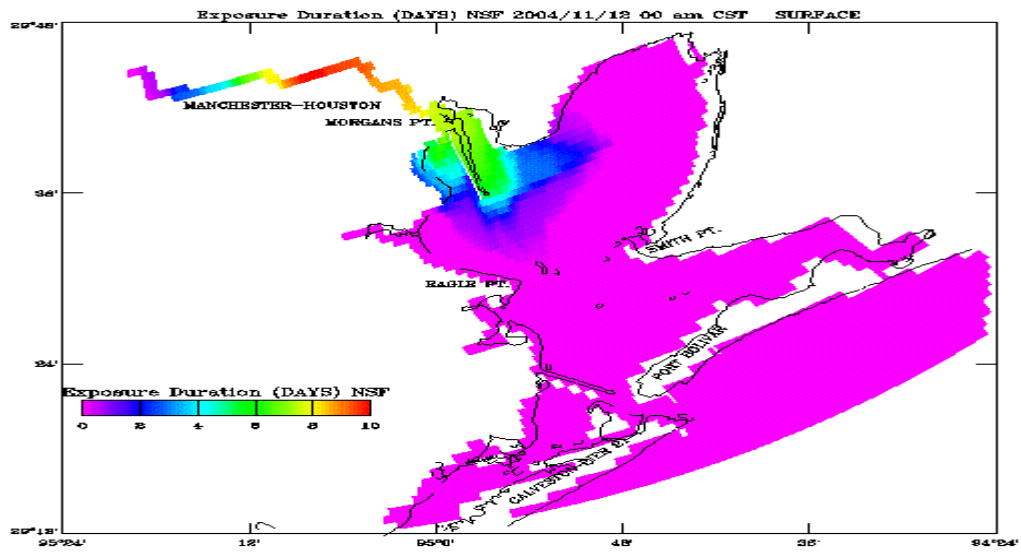


Figure 5.29. Simulated near surface no surface flux (CS2) exposure duration (days). (Upper panel GBM, Lower panel HSCM).

5.4.4. Turnover Time

With respect to the initial injection grid cell, the total turnover time is determined as the time at which the total mass is reduced by $1/e$ of the initial mass. The turnover times are given in Table 5.2 for both Bay and Channel models for each of the 5 levels as well. Note it is possible, that once the mass is reduced to $1/e$ of its initial mass, the mass may increase again. This is not indicated in the turnover time and must be determined by examining the concentration time history at the given location.

Table 5.2. SF₆ Turnover times (days). Note CS1 represents SF₆ with surface gas transfer, while CS2 represents SF₆ with no surface gas transfer and k=1 (surface),2,3,4, and 5 (bottom) sigma levels.

Parameter	Galveston Bay Model	Houston Ship Channel Model
Total (CS1,CS2)	(0.1674, 0.1708)	(0.1019,0.1030)
(CS1,CS2,k=1)	(0.1965, 0.2056)	(0.2024,0.2111)
(CS1,CS2,k=2)	(0.0701, 0.0750)	(0.0378,0.0378)
(CS1,CS2,k=3)	(0.1097,0.1486)	(0.0497,0.0496)
(CS1,CS2,k=4)	(0.1458,0.1492)	(0.0766,0.0766)
(CS1,CS2,k=5)	(0.1514,0.1555)	(0.1297,0.1300)

5.4.5. Mass Inventory

To check on the mass consistency of the computations, a mass inventory was determined at the end of the simulation. The difference in the initial mass and the sum of the final mass, mass lost through the surface, and the mass lost through the lateral boundaries was determined as the mass error. It should be noted that while the mass balance computations were carried out using double precision, the quantities making up the balance were computed based on single precision arithmetic. The mass relative error was determined as the ratio of the mass error to the initial mass and was order 10^{-7} , which represent the precision of the single precision arithmetic. Results are given in Table 5.3 for the Galveston Bay Model and in Table 5.4 for the Houston Ship Channel model computations. It is interesting to observe the difference in the results for the Bay and Channel models, particularly with respect to final mass. Note the negative mass losses through the surface for CS2 in both model computations are not theoretically possible, but are due to the single precision arithmetic. Also note that the initial mass should show no nonzero numbers after the leading 1, and again shows the limits of the single precision arithmetic. Decay coefficients are computed based on an exponential decay from initial to final mass plus surface mass loss for CS1 and from initial to final mass for CS2. The decay coefficients for the Galveston Bay Model are nearly equal, while there is an order of 3 difference for the Houston Ship Channel Model.

Table 5.3. Galveston Bay Model: SF₆ Mass inventory (10⁻³ fmoles). Initial mass at 00CST on 2 November 2004 and final mass 00CST on 12 November 2004. Note CS1 represents SF₆ with surface gas transfer, while CS2 represents SF₆ with no surface gas transfers. Note the mass balance region considered is I = (15,76), J=(79,95).

Parameter	CS1	CS2
Initial Mass	1000000034488.555	1000000034488.555
Final Mass	55303991283.367	994803495802.576
Mass lost through the surface	941127766951.415	-430414.673
Mass lost through the lateral boundaries	3568325477.928	55197231770.618
Mass error	-49224.155	-262669.966
Mass relative error to the initial mass (-)	-4.922x10 ⁻⁸	-2.627x10 ⁻⁷
Decay coefficient (days ⁻¹)	-0.00036	-0.00052

Table 5.4. Houston Ship Channel Model: SF₆ Mass inventory (10⁻³ fmoles). Initial mass at 00CST on 2 November 2004 and final mass 00CST on 12 November 2004. Note CS1 represents SF₆ with surface gas transfer, while CS2 represents SF₆ with no surface gas transfers. Note the mass balance region considered is I = (9,64), J=(174,205).

Parameter	CS1	CS2
Initial Mass	1000000034488.555	1000000034488.555
Final Mass	156231572263.406	759593945725.248
Mass lost through the surface	774541589083.615	-945999.427
Mass lost through the lateral boundaries	69227572621.036	240406536065.383
Mass error	-699479.503	498697.350
Mass relative error to the initial mass (-)	-6.994x10 ⁻⁷	4.987x10 ⁻⁷
Decay coefficient (days ⁻¹)	-0.0073	-0.0274

6. CONCLUSIONS AND FUTURE WORK

The estuarine dispersion characteristics of the Houston Ship Channel and upper Galveston Bay have been investigated by the simulated movement of SF₆ tracer at Patrick Bayou in November 2004. With the addition of two concentration subroutines (with and without surface gas transfer) to the Bay and Channel hydrodynamic models and forcing with proper boundary conditions, the models have been set up to simulate the tracer movement during 2-11 November 2004. Computed areal extents of the 10 day residence time contours for both zero and nonzero surface fluxes of SF₆ bracketed the measured SF₆ contours above background concentration and demonstrated the utility of the numerical models in planning field experiments, which will determine residence and flushing times directly from measured tracer concentration data.

The concentration subroutine approach is an effective tool for characterizing the dispersion features of a soluble substance in an estuary. For other pollutants particle tracking may be a more appropriate approach. This report only documents the model simulation of the SF₆ tracer dispersion using the concentration approach. Lagrangian trajectory modeling, as reported by Wei (1994) and Blumberg et al. (2004), could also be applied to study the SF₆ tracer dispersion experiments and compared with results from the concentration modeling. In addition, the concept of age, introduced by Deleersnijder et al. (2001) as applied by Shen and Hass (2004), could also be investigated to further characterize dispersion characteristics. The residence time estimates as studied by Wang et al. (2004) might also be tried as alternative measures as well.

Additional wave-current interaction experiments, should be conducted in which the limit on the bottom adjustment factor of 2.0 is altered. Additional work in this area, by Mellor (2003a), Johnson (1992), and Monahan (2002) should also be considered in an effort to develop an iterative approach for z_0 . It would also be of interest to compare the SWAN and simpler parametric model results to further quantify their limitations.

ACKNOWLEDGMENTS

The solute model work has been carried out in the Coast Survey Development Laboratory (CSDL) of NOS's Office of Coast Survey with the encouragement from the Chief of CSDL's Marine Modeling and Analysis Programs, Dr. Frank Aikman. Discussions with Dr. Eugene Wei regarding his work on the simulation of the SF₆ tracer in the New York Harbor have greatly assisted this work.

REFERENCES

- Blumberg, A. F., and G. L. Mellor, 1987. A description of a three-dimensional coastal ocean circulation model. *Three-Dimensional Coastal Ocean Models*, (ed. Heaps), American Geophysical Union, Washington, DC., 1 - 16.
- Blumberg, A. F., and H.J. Herring, 1987. Circulation modeling using orthogonal curvilinear coordinates, in *Three-Dimensional Models of Marine and Estuarine Dynamics*, (ed. Nihoul and Jamart), Elsevier Oceanography Series, 45, 55-88.
- Blumberg, A. F., D.J. Dunning, H. Li, S. Heimbuch, and W.R. Geyer, 2004. Use of a Particle-tracking Model for Predicting Entrainment at Power Plants on the Hudson River, *Estuaries*, Vol.

27, No. 3, 515-526.

Caplow, T., P. Schlosser, D.T. Ho, and N. Santella, 2003. Transport Dynamics in a Sheltered Estuary and Connecting Tidal Straits: SF₆ Tracer Study in New York Harbor, *Environmental Science Technology*, 37, 5116-5126.

Coastal Engineering Technical Note, CETN-I-6, 1981. Revised method for wave forecasting in shallow water, Coastal Engineering Research Center, Vicksburg, MS.

Davies, A.M. and J. Lawrence, 1995. Modeling the effect of wave-current interaction on the three-dimensional wind-driven circulation of the Eastern Irish Sea, *Journal of Physical Oceanography*, 25, 29-45.

Deleersnijder, E., J-M Campin, E.J.M. Delhez, 2001. The concept of age in marine modeling I. Theory and preliminary model results, *Journal of Marine Systems*, 28, 229-267.

Donelan, M.A., 1977: A simple numerical model for wave and wind stress prediction, *Report, National Water Resources Institute*, Burlington, Ontario.

Drennan, W.M, H.C. Graber, D. Hauser, and C. Quentin, 2003. On the wave age dependence of wind stress over pure wind seas, *Journal of Geophysical Research*, 108, 8062.

Grant, W.D and O.S. Madsen, 1979. Combined wave and current interaction with a rough bottom, *Journal of Geophysical Research*, 84, 1797-1808.

Grant, W.D. and O.S. Madsen, 1982. Movable bed roughness in unsteady oscillatory flow, *Journal of Geophysical Research*, 87, 469-481.

Ho, D.T., P. Schlosser, and T. Caplow, 2002. Determination of Longitudinal Dispersion Coefficient and Net Advection in the Tidal Hudson River with a Large-Scale, High Resolution SF₆ Tracer Release Experiment, *Environmental Science Technology*, 36, 3232-3241.

Hurdle, J.P., J.K. Kostense, and P.van den Bosch, 1989. Mild-slope model for the wave behaviour in and around harbours and coastal structures in areas of variable depth and flow conditions, In: *Advances in Water Modelling and Measurement*.

Jahne, B., K.O. Munnich, R. B. Singer, A. Dutzi, W. Huber, and P. Libner, 1987. On the Parameters Influencing Air-Water Gas Exchange, *Journal of Geophysical Research*, Vol. 92, C2, 1937-1949.

Johnson, H.K., and H.J. Vested, 1992. Effects of water waves on wind shear stress for current modeling, *Journal of Atmospheric and Oceanic Technology*, 9, 850-861.

Large, W.G. and Pond, S., 1981. Open ocean momentum flux measurements in moderate to strong winds, *Journal of Physical Oceanography*, 11, 324-336.

Mellor, G.L., 2003a. The three-dimensional, current and surface wave equation, *Journal of Physical Oceanography*, 33, 1978-1989.

Mellor, G.L., 2003b. Users guide for a three-dimensional, primitive equation, numerical ocean model, *Progr Atmos and Ocean Sci*, Princeton University. (Available at www.aos.princeton.edu/WWWPUBLIC/htdocs.pom/publications.htm)

Mellor, G. L. and A. F. Blumberg, 2004. Wave breaking and ocean surface layer thermal response, *J. Phys. Oceanogr.*, 34, 693-698.

Mellor, G. L. and M. A. Donelan, 2006. A surface wave model for coupling with numerical ocean circulation models, submitted.

Monahan E. C., 2002. Oceanic whitecaps: Sea surface features detectable via satellite that are indicators of the magnitude of the air-sea gas transfer coefficient, *Proceedings Indian Academy of Sciences, Earth and Planetary Science*, 111, No 3, 315-319.

NOS, 1999. NOS procedures for developing and implementing operational nowcast and forecast systems for PORTS, *NOAA Technical Report NOS CO-OPS 0020*, Silver Spring, MD.

NOS, 2005. Report on the National Ocean Service Workshop on Residence Time in Bays and Estuaries, NOS, CSDL, Silver Spring, MD.

Project CW-167, 1955. Waves and wind tides in shallow lakes and reservoirs: summary report, U.S. Army Corps of Engineers, Jacksonville, FL.

Ris, R.C., 1997: Spectral modelling of wind waves in coastal areas, (Ph.D. Dissertation Delft University of Technology, Department of Civil Engineering), Communications on Hydraulic and Geotechnical Engineering, Report No. 97-4, Delft, The Netherlands.

Schlosser, P., D. Ho, and P. Schmieder, SF6 Tracer Release Experiment in the Houston Ship Channel, Final Report, Lamont-Doherty Earth Observatory of Columbia University, New York, NY, June 2006.

Schmalz, R.A., 1996. National Ocean Service Partnership: DGPS-supported hydrosurvey, water level measurement, and modeling of Galveston Bay: development and application of the numerical circulation model. NOAA, National Ocean Service, Office of Ocean and Earth Sciences, *NOAA Technical Report NOS OES 012*, Silver Spring, MD.

Schmalz, R.A., 1998a. Development of a Nowcast/Forecast System for Galveston Bay, *Proceedings of the 5th Estuarine and Coastal Modeling Conference*, ASCE, Alexandria, VA, 441-455.

Schmalz, R.A., 1998b. Design of a Nowcast/Forecast System for Galveston Bay, *Proceedings of the 2nd Conference on Coastal Atmospheric and Oceanic Prediction and Process*, AMS, Phoenix, AZ, 15-22.

Schmalz, R.A., 1998c. Initial Evaluation of a Nowcast/Forecast System for Galveston Bay

during September 1997, *Proceedings of the Ocean Community Conference*, MTS, Baltimore, MD, 426-430.

Schmalz, R.A., 2000a: A Nowcast/Forecast System for Galveston Bay, *Proceedings of the 2000 Joint Conference on Water Resources Engineering and Water Resources Planning and Management*, ASCE, General Conference, Flood Hazard Modeling Applications, CDROM.

Schmalz, R.A., 2000b. Demonstration of a Nowcast/Forecast System for Galveston Bay, *Proceedings of the 6th Estuarine and Coastal Modeling Conference*, ASCE, New Orleans, LA, 868-883.

Schmalz, R.A., 2000c. High-Resolution Houston Ship Channel ADCP and CTD Survey: Model-Data Intercomparisons, *NOAA Technical Report NOS CS 6*, Silver Spring, MD.

Schmalz, R.A., 2001. Three-Dimensional Hydrodynamic Model Developments for a Galveston Bay Nowcast/Forecast System, *NOAA Technical Report NOS CS 9*, Silver Spring, MD.

Schmalz, R.A., 2003. Development of a Real Time Wave Model for Galveston Bay, *Proceedings of the World Water & Environmental Resources Congress*, ASCE, Philadelphia, PA, CDROM.

Schmalz, R.A., 2004. Development of the NOS Galveston Bay Operational Nowcast/Forecast System, *Proceedings of the 7th International Marine Environmental Modelling Seminar*, Washington, DC.

Schmalz, R.A. and P. H. Richardson, 2002. Evaluation of the NOS Experimental Nowcast/Forecast System for a Galveston Bay, *NOAA Technical Report NOS CS 14*, Silver Spring, MD.

Schwab, D. R., J.R. Bennett, P.C. Liu, and M.A. Donelan, 1984. Application of a Simple Numerical Wave Prediction Model to Lake Erie, *Journal of Geophysical Research*, Vol. 89, C3, 3586-3592.

Shen, J. and L. Haas, 2004. Calculating age and residence time in the tidal York River using three-dimensional model experiments, *Estuarine, Coastal, and Shelf Science*, 61, 449-461.

Signell, R.P., R.C. Beardsley, H.C. Graber, and A. Capotondi, 1990. Effect of wave-current interaction on wind-driven circulation in narrow, shallow embayments. *Journal of Geophysical Research*, 95, 9671-9678.

Smagorinsky, J. 1963. General circulation experiments with the primitive equations, I. The basic experiment. *Monthly Weather Review*, 91, 99-164.

Smith, S.D. 1980. Wind stress and heat flux over the ocean in gale force winds, *Journal of Physical Oceanography*, 10, 709-726.

Wang, Chi-Fang, Ming-His Hsu, and Albert Y. Kuo, 2004. Residence time of the Danshuei River estuary, Taiwan, *Estuarine, Coastal, and Shelf Science* 60,381-393.

Wanninkhof, R., 1992. Relationship Between Wind Speed and Gas Exchange Over the Ocean, *Journal of Geophysical Research*, Vol. 97, No. C5, 7373-7382.

Wei, Eugene J., 1994. Lagrangian Drifter Trajectory Modeling. *NOAA Technical Report NOS OES 004*, NOS, NOAA, Silver Spring, MD.

Wei, Eugene J., 2004. Solute Dispersion Modeling in New York Harbor. *NOAA Technical Report NOS CS 18*, NOS, NOAA, Silver Spring, MD.